ΠΑΝΕΠΙΣΤΗΜΙΟ ΠΑΤΡΩΝ

ΤΜΗΜΑ ΙΑΤΡΙΚΗΣ ΤΜΗΜΑ ΦΥΣΙΚΗΣ

ΔΙΑΤΜΗΜΑΤΙΚΟ ΠΡΟΓΡΑΜΜΑ ΜΕΤΑΠΤΥΧΙΑΚΩΝ ΣΠΟΥΔΩΝ ΣΤΗΝ ΙΑΤΡΙΚΗ ΦΥΣΙΚΗ

ΑΝΑΠΤΥΞΗ ΥΠΟΛΟΓΙΣΤΙΚΟΥ ΜΟΝΤΕΛΟΥ ΠΡΟΣΩΜΟΙΩΣΗΣ ΦΘΟΡΙΖΟΝΤΩΝ ΥΛΙΚΩΝ ΑΝΙΧΝΕΥΤΩΝ ΙΑΤΡΙΚΗΣ ΑΠΕΙΚΟΝΙΣΗΣ ΜΕ ΤΕΧΝΙΚΕΣ MONTE CARLO

ΠΑΝΑΓΙΩΤΗΣ .Φ. ΛΙΑΠΑΡΙΝΟΣ

ΔΙΔΑΚΤΟΡΙΚΗ ΔΙΑΤΡΙΒΗ

Πάτρα 2007

ΠΑΝΕΠΙΣΤΗΜΙΟ ΠΑΤΡΩΝ

ΤΜΗΜΑ ΙΑΤΡΙΚΗΣ ΤΜΗΜΑ ΦΥΣΙΚΗΣ

ΔΙΑΤΜΗΜΑΤΙΚΟ ΠΡΟΓΡΑΜΜΑ ΜΕΤΑΠΤΥΧΙΑΚΩΝ ΣΠΟΥΔΩΝ ΣΤΗΝ ΙΑΤΡΙΚΗ ΦΥΣΙΚΗ

ΑΝΑΠΤΥΞΗ ΥΠΟΛΟΓΙΣΤΙΚΟΥ ΜΟΝΤΕΛΟΥ ΠΡΟΣΟΜΟΙΩΣΗΣ ΦΘΟΡΙΖΟΝΤΩΝ ΥΛΙΚΩΝ ΑΝΙΧΝΕΥΤΩΝ ΙΑΤΡΙΚΗΣ ΑΠΕΙΚΟΝΙΣΗΣ ΜΕ ΤΕΧΝΙΚΕΣ MONTE CARLO

ΠΑΝΑΓΙΩΤΗΣ .Φ. ΛΙΑΠΑΡΙΝΟΣ

ΔΙΔΑΚΤΟΡΙΚΗ ΔΙΑΤΡΙΒΗ

Πάτρα 2007

UNIVERSITY OF PATRAS

SCHOOL OF MEDICINE DEPARTMENT OF PHYSICS

INTERDEPARTMENTAL PROGRAMME OF POSTGRADUATE STUDIES IN MEDICAL PHYSICS

DEVELOPMENT OF COMPUTERIZED SIMULATION MODEL ON PHOSPHOR MATERIALS DETECTORS OF MEDICAL IMAGING BY MONTE CARLO METHODS

PANAGIOTIS. F. LIAPARINOS

DOCTORATE THESIS

Patras 2007

THREE MEMBER ADVISORY COMMITTEE

Professor George Panayiotakis	*Supervisor*
Professor Ioannis Kandarakis	*Member of the Advisory Commitee*
Professor Dionisis Cavouras	*Member of the Advisory Commitee*

SEVEN MEMBER EXAMINATION COMMITTEE

Professor George Panayiotakis	*Supervisor*
Professor George Nikiforidis	*Member of the Examination Commitee*
Professor Nikolaos Pallikarakis	*Member of the Examination Commitee*
Professor Dimitrios Siamplis	*Member of the Examination Commitee*
Professor Pavlos Vassilakos	*Member of the Examination Commitee*
Associate Professor Alexandros Vradis	*Member of the Examination Commitee*
Assistant Professor Eleni Costaridou	*Member of the Examination Commitee*

ACKNOWLEDGEMENTS

Within the framework of my PhD discourse i would like to thank:

Professor George Panayiotakis for giving me the opportunity to carry out this thesis under his supervision, providing me advises and support.

Professor Ioannis Kandarakis for giving me the inspiration to follow this path of life, helping me in every step of it. His pure character as well as his intellectual state of mind were catalytic parameters in order to express my ideas and to love whatever I do, being always myself. His contribution is positively indescribable.

Professor Dionisis Cavouras for guiding me at the beginning in the computational part of this thesis and for his invaluable advises and support.

All those people that affected me by their own personal way.

To those who are characterized
by the will to knowledge…

ΠΕΡΙΛΗΨΗ

Οι ενδογενείς ιδιότητες των φθοριζόντων υλικών ανιχνευτών ιατρικής απεικόνισης, παίζουν πολύ σημαντικό ρόλο στην απόδοση των ενισχυτικών πινακίδων που χρησιμοποιούνται σε ιατρικά απεικονιστικά συστήματα. Σε προηγούμενες μελέτες φθοριζόντων υλικών κοκκώδους μορφής, είτε με αναλυτικές μεθόδους είτε με τεχνικές Monte Carlo, οι τιμές των οπτικών παραμέτρων καθώς και οι πιθανότητες αλληλεπίδρασης του φωτός υπολογίστηκαν με τη βοήθεια τεχνικών προσαρμογής (fitting) σε πειραματικά δεδομένα. Ωστόσο, είχε παρατηρηθεί ότι στηριζόμενοι σε πειραματικά δεδομένα και τεχνικές προσαρμογής, οι οπτικοί παράμετροι ενός συγκεκριμένου υλικού μεταβάλλονται εντός ενός σημαντικού εύρους τιμών (π.χ. είχαν δημοσιευτεί, για το ίδιο πάχος υλικού διαφορετικές τιμές ενεργούς διατομής οπτικής σκέδασης). Στην παρούσα διδακτορική διατριβή αναπτύχθηκε ένα υπολογιστικό μοντέλο προσωμοίωσης φθοριζόντων υλικών κοκκώδους μορφής, με τεχνικές Monte Carlo, με σκοπό τη μελέτη διάδοσης των ακτίνων-χ και του φωτός. Το μοντέλο στηρίχθηκε μόνο στις φυσικές ιδιότητες των φθοριζόντων υλικών. Κάνοντας χρήση της θεωρίας σκέδασης Mie και με τη βοήθεια του μιγαδικού συντελεστή διάθλασης των υλικών, χρησιμοποιήθηκαν μικροσκοπικές πιθανότητες αλληλεπίδρασης του φωτός. Η εγκυρότητα του μοντέλου πιστοποιήθηκε συγκρίνοντας αποτελέσματα (π.χ. ποσοστό απορρόφησης ακτίνων-χ, στατιστική κατανομή μετατροπής των ακτίνων-χ σε φωτόνια φωτός, αριθμός εκπεμπόμενων οπτικών φωτονίων, κατανομή του φωτός στην έξοδο του ανιχνευτή) με δημοσιευμένα πειραματικά δεδομένα για το φθορίζον υλικό Gd_2O_2S:Tb (ενισχυτική πινακίδα τύπου Kodak Min-R). Τα αποτελέσματα έδειξαν την εξάρτηση της συνάρτησης μεταφοράς διαμόρφωσης (MTF) από το μέγεθος του κόκκου και από τον αριθμό των κόκκων ανα μονάδα μάζας (πακετοποιημένη πυκνότητα: packing density). Προβλέφθηκε ότι

ενισχυτικές πινακίδες με φθορίζον υλικό υψηλού αριθμού κόκκων ανά μονάδα όγκου και χαμηλής τιμής μεγέθους κόκκου μπορούν να παρουσιάσουν καλύτερη απόδοση ως προς την ποσότητα και την κατανομή του εκπεμπόμενου φωτός σε σχέση με τις συμβατικές ενισχυτικές πινακίδες, κάτω απ'τις ίδιες πειραματικές συνθήκες (π.χ. ενέργεια ακτίνων-χ, πάχος ενισχυτικής πινακίδας).

ΘΕΩΡΗΤΙΚΟ ΜΕΡΟΣ

ΑΝΙΧΝΕΥΤΕΣ ΑΚΤΙΝΟΒΟΛΙΑΣ

Τα διαγνωστικά συστήματα ιατρικής απεικόνισης βασίζονται στην καταγραφή και αποθήκευση πληροφοριών που δίνουν στοιχεία τόσο για την ανατομία όσο και για την παθολογία του ανθρώπινου σώματος. Συγκεκριμένα, η ιονίζουσα ακτινοβολία εξασθενεί από το σώμα του ασθενούς και στη συνέχεια ανιχνεύεται με χρήση φθοριζουσών οθονών (phosphor screens) ή σπινθηριστών (scintillators) που έχουν την ιδιότητα να μετατρέπουν την ιονίζουσα ακτινοβολία σε ηλεκτρομαγνητική ακτινοβολία στην περιοχή του ορατού. Το φως που εκπέμπεται προσπίπτει στην επιφάνεια ενός οπτικού ανιχνευτή (π.χ. φιλμ, φωτοπολλαπλασιαστής) ο οποίος είναι ευαίσθητος στα μήκη κύματος του εκπεμπόμενου φωτός και οι οπτικοί φορείς πληροφορίας συμβάλουν στον σχηματισμό της ιατρικής εικόνας. Οι φθορίζουσες οθόνες ή οι σπινθιριστές χαρακτηρίζονται από παραμέτρους οι οποίες εκφράζουν την ένταση και την κατανομή του παραγόμενου σήματος στην έξοδο του ανιχνευτή και σχετίζονται άμεσα με την ποιότητα της ιατρικής εικόνας αλλά και με τη δόση ασθενούς. Οι πιο σημαντικές παράμετροι είναι οι ακόλουθες: (α) Η κβαντική ανιχνευτική αποδοτικότητα (Quantum Detection Efficiency-QDE), η οποία εκφράζει το ποσοστό της ιονίζουσας ακτινοβολίας που ανιχνεύεται από τον ανιχνευτή, (β) Η

απόδοση φωτός (Luminescence Efficiency-LE), η οποία εκφράζει την ευαισθησία του ανιχνευτή και σχετίζεται με τη φωτεινότητα της ιατρικής εικόνας, (γ) Η συνάρτηση μεταφοράς διαμόρφωσης (Modulation Transfer Function-MTF), η οποία περιγράφει τη μεταβολή του σήματος διαμόρφωσης εξόδου ως συνάρτηση της χωρικής συχνότητας και σχετίζεται με τη χωρική διακριτική ικανότητα του απεικονιστικού συστήματος και (δ) Η ανιχνευτική κβαντική αποδοτικότητα (Detective Quantum Efficiency-DQE), η οποία εκφράζει την ικανότητα του απεικονιστικού συστήματος να μεταφέρει το λόγο σήματος προς θόρυβο (Signal to Noise Ratio-SNR) και σχετίζεται με τη «χρήσιμη» πληροφορία στην ιατρική εικόνα, δηλαδή την πληροφορία με διαγνωστική αξία. Οι παραπάνω παράμετροι παίζουν καθοριστικό ρόλο στην επιλογή του ανιχνευτικού υλικού και η επιλογή ποικίλλει ανάλογα με την εφαρμογή του. Ωστόσο, παρόλη την καθιέρωση παραδοσιακών φθοριζόντων υλικών σε κλασσικά απεικονιστικά συστήματα, η μελέτη καινούργιων δομών καθώς και η εύρεση καινούργιων υλικών ανιχνευτών είναι αναγκαία για τη βελτίωση των ανιχνευτικών συστημάτων (βελτίωση ποιότητας της ιατρικής εικόνας και ελάττωση της δόσης ασθενούς).

ΤΕΧΝΙΚΕΣ MONTE ΚΑΡΛΟ

Η μέθοδος Monte Carlo είναι μια αριθμητική μέθοδος που δίνει προσεγγιστική λύση σε μαθηματικά προβλήματα με την βοήθεια της τεχνικής που ονομάζεται «τυχαία δειγματοληψία». Σε αντίθεση με τη μέθοδο Μόντε Κάρλο, οι συμβατικές αριθμητικές μέθοδοι επιδιώκουν να προσεγγίσουν την εξέλιξη των φυσικών συστημάτων περιγράφοντας τα συστήματα με μαθηματικά μοντέλα και επιλύοντας μια σειρά από αλγεβρικές εξισώσεις. Η μέθοδος Monte Carlo δεν βρίσκει εφαρμογή μόνο σε προβλήματα τα οποία ενσωματώνουν την έννοια του τυχαίου (επειδή αυτά

περιγράφονται από συναρτήσεις πυκνότητας πιθανότητας) αλλά και σε άλλα προβλήματα όπως ο υπολογισμός ενός ορισμένου ολοκληρώματος. Όμως και σε αυτές τις περιπτώσεις η λύση δίνεται μέσω κάποιας πυκνότητας πιθανότητας και το πρόβλημα αντιμετωπίζεται σαν τυχαία (στοχαστική) διαδικασία. Γενικότερα εφαρμόζεται σε κάθε πρόβλημα του οποίου η αναλυτική επίλυση είναι αδύνατη ή προϋποθέτει την εισαγωγή απλουστεύσεων. Για το λόγο αυτό, τα αποτελέσματα αυτής της μεθόδου μπορεί να υπερτερούν των αντίστοιχων αποτελεσμάτων των άλλων (αναλυτικών ή μαθηματικών) μεθόδων. Τα κύρια «εργαλεία» της μεθόδου Monte Carlo είναι τα ακόλουθα:

(α) Συνάρτηση πυκνότητας πιθανότητας. Το φυσικό ή μαθηματικό πρόβλημα πρέπει να περιγράφεται από μια σειρά συναρτήσεων πυκνότητας πιθανότητας.

(β) Γεννήτρια τυχαίων αριθμών. Πρέπει να διατίθεται μια πηγή παραγωγής τυχαίων αριθμών ομοιόμορφα κατανεμημένων στο μοναδιαίο διάστημα.

(γ) Μέθοδος δειγματοληψίας. Για τη δειγματοληψία μιας παραμέτρου θα πρέπει να επιλέγεται η κατάλληλη μέθοδος δειγματοληψίας (π.χ. μέθοδος της αντιστροφής, μέθοδος απόρριψης).

(δ) Εκτίμηση σφάλματος. Πρέπει να ορίζεται εκτίμηση του στατιστικού σφάλματος σαν συνάρτηση του αριθμού των προσομοιώσεων.

(ε) Τεχνικές ελάττωσης της σταθεράς διακύμανσης. Οι τεχνικές αυτές έχουν σκοπό την ελάττωση του χρόνου που χρειάζεται για να ολοκληρωθεί μια προσομοίωση με δεδομένη σταθερά απόκλισης της τιμής του μεγέθους που προσδιορίζεται.

ΑΝΑΠΤΥΞΗ ΜΟΝΤΕΛΟΥ

ΕΙΣΑΓΩΓΗ - ΤΟ ΠΡΟΒΛΗΜΑ

Τα απεικονιστικά χαρακτηριστικά των φθοριζουσών οθονών εξαρτώνται άμεσα τόσο από τις φυσικές ιδιότητες όσο και από τις ιδιότητες δομής του υλικού. Οι προαναφερθείσες ιδιότητες, οι οποίες έχουν μελετηθεί από πειραματικές διατάξεις, αναλυτικά μοντέλα καθώς κι από μοντέλα με τεχνικές Monte Carlo, λαμβάνονται υπόψην στο σχεδιασμό και στην κατασκευή εμπορικών απεικονιστικών συστημάτων. Από τις πρώτες μελέτες που εμφανίστηκαν να διαπαραγματεύνται τη συμπεριφορά των φθοριζουσών οθονών ήταν του Hamaker ο οποίος έδωσε υπολογισμούς εκπομπής φωτός από ένα στρώμα υλικού κάνοντας χρήση της θεωρίας διάδοσης του φωτός των Kubelca και Munk. Στην ίδια κατεύθυνση ο Ludwig έδωσε αποτελέσματα εκπομπής φωτός πολλών ενισχυτικών πινακίδων. Στην συνέχεια ο Swank μίλησε για το θόρυβο που προκύπτει από τη μεταβλητότητα των εκπεμπόμενων οπτικών παλμών. Ο Giakoumakis διαπραγματεύτηκε τους περιορισμούς των αναλυτικών μοντέλων κυρίως σε χαμηλές τιμές πάχους οθόνης και τέλος οι Nishikawa και Yaffe ανέπτυξαν ένα ολοκληρωμένο μοντέλο με το οποίο μπορούσες να προβλέψεις τα απεικονιστικά χαρακτηριστικά των φθοριζουσών οθονών που σχετίζονταν με την ποιότητα της ιατρικής εικόνας.

Όσον αφορά τα μοντέλα με τεχνικές Monte Carlo, τα περισσότερα είχαν εστιάσει στη μοντελοποίηση των ακτίνων-χ. Ο Kalender με ένα απλό μοντέλο μελέτησε τη σκέδαση των ακτίνων-χ μέσα στον ανιχνευτή και οι Chan και Doi δημοσίευσαν τεχνικές δειγματοληψίας παραμέτρων και έδωσαν ένα ολοκληρωμένο μοντέλο για τη διάδοση των ακτίνων-χ, μοντέλο που επηρέασε όλα τα εμπορικά πακέτα Monte Carlo της δεκαετίας του 90’ (π.χ. PENELOPE, GEANT4, EGS4). Ωστόσο, η διάδοση του

φωτός με τεχνικές Monte Carlo είχε μελετηθεί από τον Morlotti ο οποίος είχε κάνει μια εισαγωγή στην θεωρία σκέδασης Mie και είχε χρησιμοποιήσει οπτικές παραμέτρους από τους Kubelca και Munk. Ο Aerts είχε περιγράψει τη διάδοση του φωτός μέσω μιας ισοτροπικής κατανομής και οι Radcliffe και Kausch είχαν αναπτύξει ένα μοντέλο για την ανάκλαση του φωτός στα όρια μεταξύ των επιφανειών της οθόνης και του οπτικού αισθητήρα. Τέλος ο Badano έκανε βελτιστοποίηση οπτικών παραμέτρων συγκρίνοντας αποτελέσματα του μοντέλου του σε σύγκριση με αντίστοιχα πειραματικά δεδομένα και δεδομένα που προέκυπταν από τα αναλυτικά μοντέλα των Nishikawa και Yaffe.

Ωστόσο, σε όλες τις μελέτες, είτε με αναλυτικά μοντέλα είτε με μοντέλα Monte Carlo, είχαν δημοσιευτεί για το ίδιο υλικό διαφορετικοί οπτικές παράμετροι σκέδασης και απορρόφησης λόγω του ότι οι τιμές τους προέρχονταν από μεθόδους «ταιριάματος» (fitting) σε πειραματικά δεδομένα. Έτσι, είχε δημιουργηθεί ένα πρόβλημα που σχετιζόταν τόσο με τη μεταβλητότητα των οπτικών παραμέτρων όσο και με την εξάρτηση των μοντέλων από πειραματικές μετρήσεις. Η παρούσα διδακτορική διατριβή επιχειρεί να επιλύσει το παραπάνω πρόβλημα.

Επίσης, οι φθορίζουσες οθόνες που χρησιμοποιούνται στα ιατρικά απεικονιστικά συστήματα αποτελούνται από κόκκους υλικού οι οποίοι είναι κολλημένοι με τη βοήθεια συνδετικού υλικού. Συγκεκριμένα, ο αριθμός των κόκκων υλικού ανά μονάδα μάζας εκφράζεται από την παράμετρο «πακετοποιημένης πυκνότητας» η οποία στις συμβατικές οθόνες θεωρείται σταθερή και ίση με 50%. Ωστόσο, την τελευταία δεκαετία, έχουν αναπτυχθεί καινούργιες τεχνικές σύντηξης με τις οποίες μπορεί να επιτευχθεί αύξηση του αριθμού των κόκκων ανα μονάδα μάζας, δηλαδή αύξηση της παραμέτρου «πακετοποιημένης πυκνότητας». Η επίδραση αυτής της παραμέτρου στην απόδοση των φθοριζουσών οθονών δεν έχει μελετηθεί και στην

παρούσα διδακτορική διατριβή μελετάται αναλυτικά.

Τέλος, παρόλη την καθιέρωση παραδοσιακών φθοριζόντων υλικών σε κλασσικά απεικονιστικά συστήματα, η μελέτη καινούργιων δομών καθώς και η εύρεση καινούργιων υλικών ανιχνευτών είναι αναγκαία για τη βελτίωση των ανιχνευτικών συστημάτων (βελτίωση ποιότητας της ιατρικής εικόνας και ελάττωση της δόσης του ασθενούς).

ΜΕΘΟΔΟΛΟΓΙΑ

Στην παρούδα διδακτορική διατριβή μελετήθηκε η απόδοση των φθοριζουσών οθονών ανιχνευτών ιατρικής απεικόνισης. Η μελέτη επιτεύχθηκε με την ανάπτυξη ενός υπολογιστικού μοντέλου στην πλατμόρμα MATLAB κάνοντας χρήση τεχνικών Monte Carlo. Το μοντέλο εξαρτάται μόνο από τις φυσικές ιδιότητες του υλικού (π.χ. συντελεστής διάθλασης, μήκος κύματος φωτός) και τις ιδιότητες δομής της οθόνης (π.χ. μέγεθος κόκκου, κατανομή κόκκων). Πιο συγκεκριμένα, περιλαμβάνει αναλυτικά την προσομοίωση των ακόλουθων φυσικών φαινομένων και μηχανισμών: (α) Την εναποθέτηση της ενέργειας ιονίζουσας ακτινοβολίας μέσω της εξασθένησης των ακτίνων-χ. Λήφθησαν υπόψην η ελαστική σκέδαση, η ανελαστική σκέδαση, η φωτοηλεκτρική απορρόφηση, η παραγωγή K-χαρακτηριστικής ακτινοβολίας και η εκπομπή ηλεκτρονίων Auger. (β) Την παραγωγή του φωτός ανά απορροφούμενη μονάδα ενέργειας ιονίζουσας ακτινοβολίας και (γ) Την εξασθένηση των οπτικών φωτονίων με τους κόκκους του υλικού. Η εξασθένηση του φωτός (απορρόφηση και σκέδαση) περιγράφτηκε με τη βοήθεια της θεωρίας σκέδασης Mie και την κατανομή Henyey-Greenstein. Η θεωρία σκέδασης Mie δίνει μια ολοκληρωμένη λύση των εξισώσεων του Maxwell για σκέδαση του φωτός από σωματίδια σφαιρικού σχήματος.

Σε αντίθεση με την σκέδαση Rayleigh αποδίδει καλύτερα για σωματίδια μεγέθους ίσου ή μεγαλύτερου του μήκους κύματος φωτός.

Το μοντέλο εισήγαγε τη συνεισφορά του μιγαδικού συντελεστή διάθλασης στη διάδοση του φωτός. Ο συντελεστής αυτός συνδέεται άμεσα με την πιθανότητα οπτικής σκέδασης και απορρόφησης που με τη σειρά τους εξαρτώνται από το μέγεθος του κόκκου και το μήκος κύματος φωτός. Επομένως, με αυτόν τον τρόπο δημιουργήθηκε ένα μοντέλο το οποίο μπορεί να προβλέψει τα απεικονιστικά χαρακτηριστικά (π.χ. QDE, MTF, DQE) των ανιχνευτών χωρίς την ανάγκη πειραματικών μετρήσεων. Το μοντέλο εφαρμόστηκε καταρχάς για τη μελέτη απόδοσης της εμπορικής κασσέτας Kodak Min-R υλικού Gd_2O_2S: Tb και συνέχεια για μελέτη καινούργιων φθοριζόντων υλικών (π.χ. Lu_2SiO_5:Ce).

ΑΠΟΤΕΛΕΣΜΑΤΑ-ΣΥΜΠΕΡΑΣΜΑΤΑ

Η πιστοποίηση του μοντέλου πραγματοποιήθηκε αρχικά με την επαλήθευση των κατανομών και των παραμέτρων που πηγάζουν από τις τεχνικές δειγματοληψίας παραμέτρων. Όλες οι κατανομές και οι παράμετροι επαληθεύτηκαν από τις θεωρητικές καμπύλες και τις θεωρητικές τιμές. Όσον αφορά τα μακροσκοπικά αποτελέσματα που σχετίζονται με τις παραμέτρους εξόδου του μοντέλου βρέθηκαν τα παρακάτω αποτελέσματα:

- Τα αποτελέσματα του μοντέλου, σε σύγκριση με πειραματικά αποτελέσματα, ως προς την παράμετρο QDE βρέθηκαν να αποκλίνουν κατά 0.5%.
- Τα αποτελέσματα του μοντέλου, σε σύγκριση με πειραματικά αποτελέσματα, ως προς την παράμετρο MTF βρέθηκαν να αποκλίνουν κατά 1%.
- Η συμφωνία των αποτελεσμάτων του μοντέλου σε σύγκριση με πειραματικά αποτελέσματα ως προς τις παραμέτρους LE και DQE βρέθηκε πολύ καλή.

- Η παράμετρος MTF βελτιώνεται όσο μειώνεται το μέγεθος του κόκκου.
- Η παράμετρος MTF βελτιώνεται όσο αυξάνει ο αριθμός των κόκκων ανα μονάδα μάζας.
- Οι οθόνες με υψηλή τιμή αριθμού κόκκων ανα μονάδα μάζας και χαμηλής τιμής μεγέθους κόκκου παρουσιάζουν βελτιωμένη την παράμετρο MTF ενώ ταυτόχρονα εκπέμπουν μεγαλύτερη ποσότητα φωτός σε σχέση με τις συμβατικές οθόνες.
- Βρέθηκε ότι το υλικό Lu_2SiO_5: Ce αποδίδει καλύτερα ως προς τη παράμετρο DQE σε σύγκριση με το ευρέως γνωστό και χρησιμοποιούμενο φθορίζον υλικό Gd_2O_2S: Tb.

Με βάση τη μεθοδολογία και τα αποτελέσματα της διδακτορικής διατριβής πηγάζουν τα ακόλουθα συμπεράσματα: (α) Το μοντέλο μπορεί να προβλέψει την απόδοση των φθοριζουσών οθονών χωρίς την ανάγκη πειραματικών μετρήσεων. (β) Το μοντέλο υπερτερεί αντίστοιχων αναλυτικών μοντέλων κυρίως σε χαμηλές τιμές πάχους λόγω των περιορισμών των τελευταίων σε αυτές τις συνθήκες. (γ) Οι οθόνες με υψηλή τιμή αριθμού κόκκων ανα μονάδα μάζας και χαμηλής τιμής μεγέθους κόκκου υπερτερούν των καθιερωμένων τεχνικών (π.χ. τοποθέτηση απορροφητικών βαφών) για βελτίωση της παραμέτρου MTF και (δ) Οι οθόνες υλικού Lu_2SiO_5:Ce μπορούν να χρησιμοποιηθούν σε ιατρικά συστήματα μαστογραφικής απεικόνισης.

ΠΕΡΙΟΡΙΣΜΟΙ ΚΑΙ ΜΕΛΛΟΝΤΙΚΗ ΔΟΥΛΕΙΑ

Η παρούσα διδακτορική διατριβή διαπραγματεύτηκε την συμπεριφορά φθοριζόντων υλικών ανιχνευτών ιατρικής απεικόνισης κάνοντας χρήση των τεχνικών

Monte Carlo. Ανεξάρτητα από την πιστοποίηση και την απόδοση του μοντέλου είναι σημαντικό να αναφερθεί ότι η ακρίβεια των αποτελεσμάτων σχετίζεται άμεσα από τους ακόλουθους περιορισμούς και παραδοχές, όπως: (α) η εξάρτηση του μοντέλου από δεδομένα ληφθέντα από τη διεθνή βιβλιογραφία τα οποία εμπεριέχουν αποκλίσεις, (β) η θεώρηση κατανομής Poisson για την παραγωγή οπτικών φωτονίων για κάθε απορροφούμενο φωτόνιο-χ, (γ) η δέσμη του παραγόμενου φωτός θεωρήθηκε μονοχρωματική, (δ) το φανταστικό μέρος του μιγαδικού συντελεστή διάθλασης θεωρήθηκε να είναι της τάξης του 10^{-6} και (ε) η προσομοίωση των ηλεκτρονίων δεν λήφθηκε υπόψην.

Ως μελλοντική εργασία, μετά την ολοκλήρωση της διδακτορικής διατριβής, επισημαίνονται παρακάτω τα πιο σημαντικά και ενδιαφέροντα θέματα, όπως: (α) Η βελτίωση του μοντέλου ως προς τους περιορισμούς και τις παραδοχές του, (β) η μελέτη καινούργιων δομών φθοριζόντων υλικών, (γ) η μελέτη καινούργιων υλικών ανιχνευτών ιατρικής απεικόνισης και (δ) η μελέτη των παραπάνω με βάση άλλες παραμέτρους, οι οποίες δεν διαπραγματεύτηκαν στην παρούσα διδακτορική διατριβή (π.χ. θόρυβος δομής υλικών).

ABSTRACT

The intrinsic phosphor properties are of significant importance for the performance of phosphor screens used in medical imaging systems. In previous analytical-theoretical and Monte Carlo studies on granular phosphor materials, values of optical properties and light interaction cross sections were found by fitting to experimental data. These values were then employed for the assessment of phosphor screen imaging performance. However, it was found that, depending on the experimental technique and fitting methodology, the optical parameters of a specific phosphor material varied within a wide range of values, i.e. variations of light scattering with respect to light absorption coefficients were often observed for the same phosphor material. In this study, x-ray and light transport within granular phosphor materials were studied by developing a computational model using Monte Carlo methods. The model was based on the intrinsic physical characteristics of the phosphor. Input values required to feed the model can be easily obtained from tabulated data. The complex refractive index was introduced and microscopic probabilities for light interactions were produced, using Mie scattering theory. Model validation was carried out by comparing model results on x-ray and light parameters (x-ray absorption, statistical fluctuations in the x-ray to light conversion process, number of emitted light photons, output light spatial distribution) with previous published experimental data on Gd_2O_2S:Tb phosphor material (Kodak Min-R screen). Results showed the dependence of the modulation transfer function (MTF) on phosphor grain size and material packing density. It was predicted that granular Gd_2O_2S:Tb screens of high packing density and small grain size may exhibit considerably better resolution and light emission properties than the conventional Gd_2O_2S:Tb screens, under similar conditions (x-ray incident energy, screen thickness).

CHAPTER A

INTRODUCTION

The only reason to adopt the term "scientific" is for fighting against dogmatism and propaganda

A.1 The problem

Luminescent materials are employed as radiation to light converters in detectors of medical imaging systems (Knoll 1989, Johns and Cunningham 1983, Yaffe 2000). In x-ray projection imaging, a large number of such materials have been employed in the form of granular screens (Blasse and Grabmaier 1994), often referred to as phosphor screens, consisting of a large number of grains embedded within a binding material. The x-ray detection and imaging performance of phosphor screens are affected by intrinsic physical properties, related to x-ray and light photon transport through the material. These properties have been previously investigated by experimental (Alig and Bloom 1977, Derenzo et al 1990, Van Eijk 2001, Dick and Motz 1981a, Dick and Motz 1981b, Ginzburg and Dick 1993, Venema 1979), theoretical (Venema 1979, Chan and Doi 1983a, Nielsen and Carlson 1984, Nishikawa and Yaffe 1990, Kandarakis et al 1997) and Monte Carlo methods (Raeside 1976, Rubinstein 1981, Morin 1988, Andreo 1991, Kalender 1981, Chan and Doi 1983b, Aerts et al 1982), and have been taken into account in the design of commercial imaging systems (Yaffe and Rowlands 1997, Gruner et al 2002, Van Eijk 2005).

Phosphor screens have been previously (Chan and Doi 1983a, Nishikawa and Yaffe 1990, Kandarakis et al 1997, Hamaker 1947, Ludwig 1971, Ludwig and Prener 1972, Swank 1974, Giakoumakis et al 1980) modelled as a series of superimposed x-ray absorbing, light creating and light attenuating elementary thin layers within the framework of cascaded linear systems analysis. Analytical methods, based on photon diffusion equations or on one-dimensional light transport considerations (Nishikawa and Yaffe 1990, Kandarakis et al 1997, Hamaker 1947, Ludwig 1971, Ludwig and Prener 1972, Swank 1974), have been preferably employed to investigate phosphor intrinsic properties. Analytical and recursive methods have also been used to model

phosphor screens as an ensemble of grains of specific size (Lindstrom and Carlsson 1999, Giakoumakis et al 1991). On the other hand, most Monte Carlo studies (Kalender 1981, Chan and Doi 1983b, Boone and Seibert 1999, Jaffray et al 1995, Gallas et al 2004) have focused on the simulation of x-ray interactions within the phosphor's mass, mainly using available Monte Carlo simulation packages (Boone and Seibert 1999, Jaffray et al 1995, Gallas et al 2004). Only a few Monte Carlo studies have investigated or have taken into consideration the effects of phosphor screen light transport properties. Morlotti (1975) has employed Monte Carlo methods to evaluate the emission efficiency and the modulation transfer function of phosphor screens by taking into consideration light propagation effects. Radcliffe et al.(1993) and Kausch et al.(1999) have studied light transport in phosphor screens for portal imaging applications. They have used a Monte Carlo code, based on Fresnell reflection at phosphor grain boundaries. Most recently, Badano et al.(2004) have used light attenuation (scattering and absorption) coefficients to study, via the DETECT II Monte Carlo simulation code, the signal and noise transfer and the so-called Lubberts effect in columnar and granular screens. In all these studies, light propagation has been examined using optical parameters determined either by empirical methods or by fitting to experimental data. (Nishikawa and Yaffe 1990, Kandarakis et al 1997, Hamaker 1947, Ludwig 1971, Ludwig and Prener 1972, Swank 1974, Giakoumakis et al 1980, Badano et al 2004). This may be inconvenient, since for predicting the performance of a phosphor material one has to prepare screens and perform measurements or, otherwise, to use experimental data obtained by others on already prepared screens.

In currently employed granular screens, phosphor grains are glued together by a binding material in a close packed spatial distribution. This distribution is described

by the screen packing density, expressing the active phosphor volume over the total screen volume, which in conventional screens is of the order of 50%. However, in the last decade, new performance boosting phosphor screen preparation techniques have been introduced, such as sintering techniques, for preparing ceramic plates that in effect increase the densification (packing density) in luminescent materials (Blasse and Grabmaier 1994, Nagarkar et al 2004). To our knowledge, the influence of that higher packing density on the imaging performance of phosphor screens has not yet been investigated systematically.

A.2 Thesis originality

In the present study, phosphor screen performance was investigated under diagnostic radiology conditions utilizing a custom Monte Carlo simulation code developed in MATLAB. The latter only requires, as input data, standard reference tabulated data of the phosphor material's intrinsic parameters (x-ray interaction parameters, x-ray to light conversion efficiency, light wavelength, complex refractive index) and structural parameters (grain size and packing density). In particular, the simulation code was developed by performing a detailed account of: (i) The energy deposition, and the corresponding contribution to light generation, from the x-ray photon interactions within the diagnostic energy range. This account comprised the elastic and inelastic scattering effects as well as the photoelectric effect including the emission of K x-rays or Auger electron for energies above the K-absorption edge. (ii) The light generation and the interactions of light photons with the phosphor grains, based on the scattering theory of Mie (Bohren and Huffman 1983, Van de Hust 1957). The model takes into account the contribution of the complex refractive index of the phosphor material in light propagation. This index is closely related to the

microscopic light interaction probabilities, which in turn are functions of particle (phosphor grain) size and light wavelength. The model can predict phosphor performance solely by Monte Carlo simulation, without having to prepare screens and perform measurements or use experimental data obtained by others.

The proposed Monte Carlo model was applied to simulate the performance of the well known commercial, Gd_2O_2S: Tb based, Kodak Min-R screen. For this screen, the variation of the x-ray absorption and the light emission properties with x-ray energy were found. Data related to the contribution of each physical process to the emitted light were also derived. The modulation transfer function (MTF) of the screen was predicted and the effect of grain size and phosphor packing density on MTF was studied. Results were validated with respect to previous experimental measurements, under similar conditions (Dick and Motz 1981b, Nishikawa and Yaffe 1990). In addition, the noise associated with the x-ray to light conversion process, quantified in the Swank factor (Dick and Motz 1981a, Dick and Motz 1981b, Ginzburg and Dick 1993, Swank 1974) was taken into account and the corresponding detective quantum efficiency (DQE) was estimated. Finally, a suitable combination of grain size and packing density is proposed, for which the resolution and light emission properties of granular phosphor screens (e.g. Gd_2O_2S: Tb) become higher, under similar conditions.

The originality of this thesis consists in:

- The development of a computational program in MATLAB platform. The program models the radiation transport as well as the light diffusion within the granular phosphor screens depending only on their physical and structural properties.

- The model of light propagation was based on Mie scattering theory and Henyey-Greenstein distribution by introducing the significance of complex refractive index of the phosphor material. Within this treatment, microscopic probabilities of light absorption and light scattering were used. The model was depended only on the physical properties (e.g. refractive index, light wavelength) as well as on the structural properties (e.g. grain size, packing density) of phosphor screens.
- The model can predict the imaging characteristics of phosphor screens i.e.: (a) the Modulation Transfer Function (MTF) (b) the Light Efficiency (LE) (c) the Swank Factor (SF) and (d) the Detective Quantum Efficiency (DQE), without the need of preparing screens and performing measurements or, otherwise, to use experimental data obtained by others on already prepared screens.
- The model showed the variation of the MTF with respect to the packing density of the phosphor screen. It was found that MTF increases as packing density increases.
- Previous analytical models, based on diffusion equation, can not accurately describe the performance of thin screens and corresponding results are of limited accuracy. The present study attempts to overcome these limitations. The light spatial distribution at screen output can be predicted and information of phosphor screen performance for different virtual experimental setups can be extracted.
- The present model predicted that granular screens of higher packing density and lower grain size were found to present considerably better light emission and spatial resolution properties in comparison with conventional screens,

under similar conditions. This may provide an advantage over techniques based on absorbing dyes incorporation for screen resolution improvement.

A.3 Publications

This work resulted in publications in international journals, and parts of it have been presented in national and international conferences.

Publications in peer reviewed scientific journals

- P. Liaparinos, I. Kandarakis, D. Cavouras, H. Delis, G. Panayiotakis. 'Modeling granular phosphor screens by Monte Carlo methods', Med. Phys. 33 (2006) 4502-4514.
- P. Liaparinos, I. Kandarakis, D. Cavouras, H. Delis, G. S. Panayiotakis. 'Investigating the effect of K-characteristic radiation on the performance of nuclear medicine scintillators by Monte-Carlo methods', Nucl. Instr. Meth. A. 569 (2006) 355-358.
- P. Liaparinos, I. Kandarakis, D. Cavouras, H. Delis, and G. Panayiotakis. 'Evaluating the radiation detection of the RbGd2Br7:Ce scintillator by Monte-Carlo methods', Nucl. Instr. Meth. A. 569 (2006) 364-367.
- P. Liaparinos, I. Kandarakis, D. Cavouras, H. Delis, G. Panayiotakis. "Monte Carlo study on the imaging performance of powder Lu_2SiO_5: Ce phosphor screens under x-ray excitation: Comparison with Gd_2O_2S:Tb screens", Med. Phys., accepted.

- P. Liaparinos, I. Kandarakis, D. Cavouras, N. Kalivas, H. Delis, G. Panayiotakis. "Evaluation of high packing density powder x-ray screens by Monte Carlo methods", Nucl. Instr. Meth. A., accepted.

Publications in international scientific conference proceedings with referees

- P. Liaparinos, I. Kandarakis, D. Cavouras, D. Nikolopoulos and G. Panayiotakis. 'Simullating the emission efficiency and resolution properties of fluorescent screens by Monte Carlo methods'. IEEE NSS/MIC/SNPS and RTSD. Rome 2004, Italy.
- P. Liaparinos, D. Cavouras, I. Kandarakis, D. Nikolopoulos and G. Panayiotakis. 'Prediction of imaging scintillator properties by Monte Carlo methods'. 4rd European Symposium on Biomedical Engineering, Patras 2004, Greece. Proceedings session 4.
- Panagiotis F. Liaparinos, Dionisis A. Cavouras, Dimitris N. Nikolopoulos, Ioannis S. Kandarakis and George S. Panayiotakis. 'Monte Carlo study on imaging parameters of Gd_2O_2S: Tb scintillator for mammographic applications'. 1st International conference 'from scientific computing to computational engineering', Athens 2004, Greece.
- P. F. Liaparinos, I.S. Kandarakis, D. A. Cavouras, H. B. Delis, G.S. Panayiotakis. 'Monte Carlo Study of Phosphor Screens Resolution Properties'. 1st International Conference on Experiments/Process/System Modelling/Simulation/Optimization (1st IC-EpsMsO), Athens 2005, Greece.

- P. Liaparinos, I. Kandarakis, D. Cavouras, H. Delis and G. Panayiotakis. 'Investigating the modulation transfer function of granular phosphor screens using Monte Carlo simulation'. 14th International Conference of Medical Physics, Nuremberg 2005, Germany.
- Liaparinos P., Kandarakis I., Cavouras D., Panayiotakis G., 'Examining the luminescence performance of granular phosphor screens'. 2st International Conference "From Scientific Computing to Computational Engineering" (2nd IC-SCCE), Athens 2006, Greece

Publications in national scientific conference proceedings with referees

- P. Liaparinos, I. Kandarakis, D. Cavouras, G. Kontaxakis, A. Santos and G. Panayiotakis. 'The effect of K x-ray photons on nuclear medical detectors'. Congreso Anual de la Sociedad Espanola de Ingenieria Biomedica, Madrid 2005, Spain.

Abstracts in international scientific conferences

- P. Liaparinos, I. Kandarakis, D. Cavouras, D. Nikolopoulos, G. Panayiotakis. 'Monte Carlo study on radiation absorption properties of Gd_2O_2S, CsI, LSO, $CaWO_4$ phosphor screens for mammographic x-ray imaging'. European Congress of Radiology, Vienna 2005, Austria.
- P. Liaparinos, I. Kandarakis, D. Cavouras, H. Delis, and G. Panayiotakis. 'Evaluating the radiation detection and light emission properties of the RbGd2Br7:Ce scintillator by Monte-Carlo methods', 3rd International

Conference on Imaging Technologies in Biomedical Sciences (ITBS2005), Milos 2005, Greece.

- P. Liaparinos, I. Kandarakis, D. Cavouras, H. Delis, G. S. Panayiotakis. 'Investigating the effect of K-characteristic radiation on the performance of nuclear medicine scintillators by Monte-Carlo methods', 3rd International Conference on Imaging Technologies in Biomedical Sciences (ITBS2005), Milos 2005, Greece.
- P. Liaparinos, I. Kandarakis, D. Cavouras, N. Kalivas, H. Delis, G. Panayiotakis. "Evaluation of high packing density powder x-ray screens by Monte Carlo methods", 10th International Symposium on Radiation Physics (ISRP-10), Coimbra 2006, Portugal

A.4 Financial support

- This work was financially supported by the Greek Ministry of Education (through EPEAEK 'Archimidis I').
- This work has been partly supported by a Fellowship from the Marie Curie Training Site REPRAMED (HPMT-CT-2001-00420, European Commission).

CHAPTER B

THEORETICAL BACKGROUND

History protects us from historicism: that thing which calls the past to solve problems in present

B.1 Monte Carlo methods

B.1.1 Introduction

Simulation is generally defined as the technique of performing sampling experiments on the model of a system. This general definition is often called definition in a wide sense, whereas simulation in a narrow sense, or stochastic simulation, is defined as experimenting with the model over time (it includes sampling stochastic variables from probability distribution). Therefore stochastic simulation is actually a statistical sampling experiment with the model. This sampling involves all the problems of statistical design analysis. Since sampling from particular distribution involves the use of random numbers, stochastic simulation is sometimes called Monte Carlo simulation. Historically, the Monte Carlo method was considered to be a technique, using random or pseudorandom numbers, for solution of a model (Rubinstein 1981).

The Monte Carlo technique of radiation transport consists of using knowledge of probability distributions governing the individual interactions of electrons and photons to simulate their transport through matter. The resultant distributions of physical quantities of interest from a large number of simulated particles (called "histories"), provides a description on the average transport properties and the associated distributions. Since the Monte Carlo method uses well-established physics principles describing the nature of the interactions, the technique assures accurate results if the code is implemented correctly and enough histories are run.

B.1.2 Sampling techniques

In this section we consider some procedures for generating ***random*** variables from different distributions. These procedures are based on the following two methods: (a) Inverse method, and (b) Acceptance-rejection method.

B.1.2.1 Inverse method

Let X be a random variable with cumulative probability distribution function (CDF.) F_x (x). To get a value, say x, of a random variable X, obtain a value, say u, of a random variable U, compute $F_x^{-1}(u)$, and set it equal to x (see Figure 1).

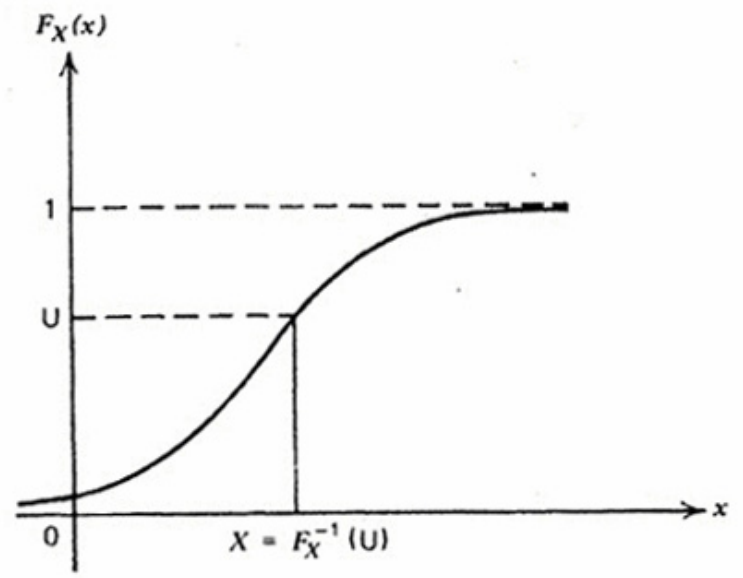

Figure 1. Inverse method

More specific the algorithm of the inversion technique can be described with the following steps (Rubenstein 1981):

Let f(x) be a PDF, x € [a, b]

- Check if f(x) is normalized: $\int_a^b f(x)dx = 1$

- Calculate the Cumulative Distribution Function: F(x) = $\int_a^x f(x)dx$
- Generate random number R
- Let F(x)=R and solve for x: $x=F^{-1}(R)$

B.1.2.2 Acceptance-rejection method

This method consists of sampling a random variable from an appropriate distribution and subjecting it to a test in order to determine whether or not it will be acceptable for use. Let [a, b] be the allowed range of values of the variable x, and p_{max} the maximum of the density p(x) (see Figure 2).

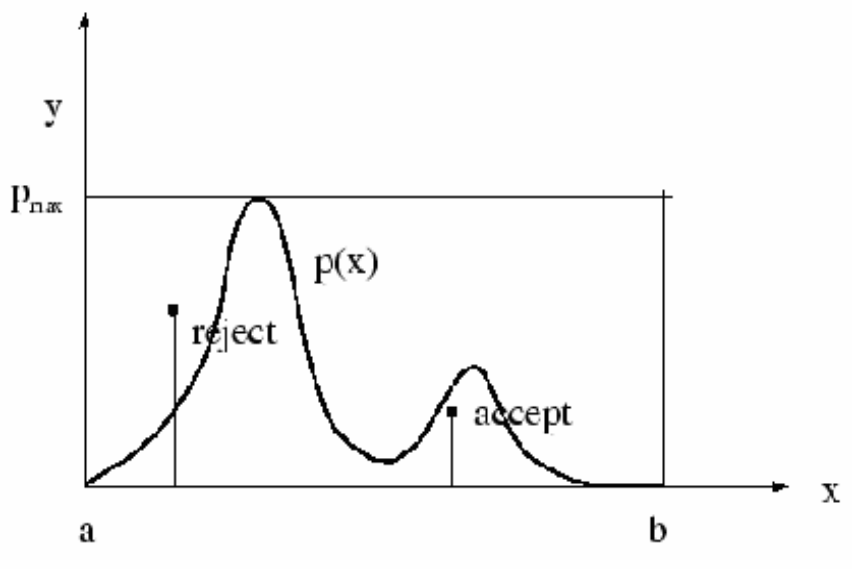

Figure 2. Rejection method

The algorithm of the acceptance-rejection method can be described with the following steps:

Let f(x) be a PDF, x € [a, b]

- Set g: $g(x)=f(x)/ p_{max}$
- Generate a random number R_1 € [0, 1).
- Generate a random value of x€ [a, b], say $x^*=a+(b-a) R_1$.

- Generate a random number R_2 € [0, 1).
- Compare R_2 with $g(x^*)$:

  If $g(x^*) \leq R_2$ then Reject x^*, otherwise Reject x^*. Return to the third step.

B.2 Phosphor screens in x-ray medical imaging

B.2.1 Introduction

Phosphor screen are employed in most of the current medical diagnostic imaging modalities using x-rays. This is explained by the comparatively good detection efficiency of phosphor screens for hard radiation. Yet, the various diagnostic methods differ considerably and consequently the radiation requirements also differ. These requirements are not always met by the phosphor screen specifications. New, digital diagnostic systems with an excellent image quality and a short image acquisition time and excellent quality real-time imaging systems for interventional radiology at a low radiation dose are two main reasons for continuous scintillator search (Johns and Cunningham 1983, Knoll 1989).

B.2.2 X-ray imaging

In x-ray radiography (static imaging) an attenuation profile of a part of the human body is projected onto a two-dimensional position-sensitive radiation detector (PSD) using the focus of an x-ray tube as a point source. Thus, information on anatomical detail is obtained. A variety of radiation detectors are used. For example, at present, for chest radiography x-ray phosphor-screen-film cassettes, typically of 35x43 cm^2, are applied as the PSD on a large scale. In most cases Gd_2O_2S:Tb is used as the x-ray intensifying screen phosphor. Furthermore, a digital chest-radiography system is used

based on the electrostatic read-out of a drum covered with an amorphous-selenium (a-Se) semiconductor layer as the PSD. Recently, new digital radiography (DR) systems have been introduced employing an a-Se photoconductor layer deposited on top of an amorphous-silicon (a-Si:H) thin-film transistor array or employing a Gd_2O_2S:Tb phosphor screen deposited on top of an array of a-Si:H photodiodes coupled to an array of thin-film transistors.

In mammography film-screen cassettes of 18x24 cm^2 are generally used. In this case a resolution of 0.1 mm is required to observe micro calcifications. Conventional film-screens systems usually consist of two equal phosphor-binder layers (thickness up to 0.3 mm per layer) and two equal emulsion layers, one on each side of the film base. More advanced systems for chest radiography are asymmetric in structure, i.e. the two screens have different thicknesses and the two emulsions are of different contrast. In mammography only one relatively thin screen (0.07 mm) and one emulsion are used to realize the required resolution (Van Eijk 2002, Yaffe and Rowlands 1997).

B.2.3 The overall performance of phosphor screens

The overall performance of phosphor screens is related to the x-ray absorption as well as the light emission properties of the screens. These properties are associated with the following imaging parameters: (a) The Quantum Detection Efficiency (QDE), (b) The Energy Absorption Efficiency (EAE), (c) The Luminescence Efficiency (LE), (d) the Modulation Transfer Function (MTF), (e) the Swank Factor and (f) the Detective Quantum Efficiency (DQE).

B.2.3.1 Quantum Detection Efficiency (QDE)

The QDE expresses the fraction of incident x-ray photons detected by a phosphor screen (Yaffe and Rowland 1997):

$$QDE(E,T) = 1 - \exp\left[-\frac{\mu(E)\rho_P}{\rho} T \right] \quad (1)$$

where $\frac{\mu(E)}{\rho}$ is the mass attenuation coefficient of the phosphor material, ρ_P is the packing density and T is the phosphor screen's coating thickness. Commercial screens used in x-ray medical imaging are usually prepared with thickness ranging from 10 mg/cm^2 up to 200 mg/cm^2 (lower values correspond to low sensitivity screens while higher values correspond to low resolution screens). In the present study two thickness values were considered: 34 mg/cm^2 corresponding to x-ray mammography and 60 mg/cm^2 corresponding to general x-ray radiography (Yu et al, 1997). QDE was estimated as the fraction of incident x-ray photons interacting within the screen. In this case, for energies lower than the K-shell binding energy, QDE is slightly higher than EAE. When an x-ray undergoes scattering and then escapes the screen, this event is taken into account in QDE evaluation while it is not included in the estimation of EAE. The latter is defined as the fraction of x-ray energy absorbed locally at the points of primary photon interactions within the phosphor mass. However the net amount of energy deposited in the screen is generally affected by: (a) the energy loss when an x-ray photon undergoes inelastic scattering and escapes phosphor mass and (b) the energy absorbed within the screen through *K* x-rays after the *K*-fluorescence emission.

B.2.3.2 Luminescence Efficiency (LE)

The LE is often ascribed to the ratio of light output over the amount of radiation incident on a phosphor or a scintillator (Ludwig 1971). It may concern either photon counting or energy integrating detectors. In the latter case, the definition of the LE can be given according to the following equation:

$$LE = \frac{\Psi_\lambda(E)}{\Psi_x(E)} \tag{2}$$

where $\Psi_\lambda(E)$ is the light energy fluence emitted by the phosphor material and $\Psi_x(E)$ is the incident x-ray energy fluence. $\Psi_\lambda(E)$ may be evaluated by taking into account the phosphor's optical spectrum $S_P(E_\lambda)$ (i.e. number of light photons per energy interval). In such a case $\Psi_\lambda(E)$ may be expressed as follows:

$$\Psi_\lambda(E) = \int_{E\lambda_2}^{E\lambda_1} S_P(E_\lambda) E_\lambda dE_\lambda \tag{3}$$

where E_λ is the light photon energy. However it has previously been assumed that, if monochromatic emission is considered, the resulting error is less than 5% (Nishikawa and Yaffe 1990). Hence all light photons may be considered to have equal energy, $E_\lambda = \overline{E_\lambda}$, i.e. the mean spectrum energy $\overline{E_\lambda}$. In this case, the light fluence is obtained by multiplying the number of the emitted light photons (N_λ) by their mean energy. N_λ is the number of light photons escaping the screen, either in reflection

(from the x-ray irradiated surface) or in transmission mode (non-irradiated surface). The incident x-ray energy fluence, $\Psi_x(E)$, is expressed by the following equation:

$$\Psi_x(E) = \int_0^{E_0} N_X(E) E dE \tag{4}$$

where E_O is the maximum spectral energy and $N_X(E)$ is the x-ray energy spectrum. The contribution of the principal intrinsic physical processes on the overall luminescence efficiency of a phosphor screen has been expressed by the following relation (Ludwig 1971, Kandarakis et al 1997):

$$LE(E,T) = n_A(E,T)\eta_c G_L(E,T) \tag{5}$$

where n_A is the absorption efficiency (i.e. corresponding to the total energy deposited within the screen), η_C is the intrinsic x-ray to light conversion efficiency, expressing the fraction of absorbed x-ray energy that is converted into light in the phosphor material (Blasse 1994) and G_L is the light transmission efficiency, i.e. the fraction of light produced that reaches the screen output (Kandarakis et al 1997). G_L also expresses how efficiently light propagates through the phosphor mass. Light propagation depends on the interactions of light photons with the phosphor grains and on the direction that light photons follow after a scattering event.

B.2.3.3 Modulation Transfer Function (MTF)

The modulation transfer function (MTF) expresses the signal transfer characteristics of an intensifying screen. The shape of the MTF curve is affected by the depth of the x-ray interaction, which in turn affects the spatial distribution of the points of light creation within the phosphor (Nishikawa and Yaffe 1990). The relative depth distribution of the absorbed x-ray energy depends on the effective atomic

number as well as on the density of the material. The contribution of scattering events (elastic or inelastic) is also included in the aforementioned consideration (Giakoumakis et al 1980). In addition to x-ray penetration, the role of light propagation is also of crucial importance since it determines the spatial distribution of the emitted light.

The MTF metric expresses the spatial resolution characteristics of an imaging system. It is defined as the ratio of the modulation of the output signal over the modulation of a sinusoidal input signal of the same frequency, given by (Yaffe, 2000):

$$MTF(u) = \frac{|T(u)|}{T(0)} \tag{6}$$

where the factor $T(u)$ is called the characteristic function of the system and $MTF(u)$ has by definition a value of unity at $u = 0$.

To predict the MTF of a phosphor screen by our Monte Carlo simulation model, pencil beam geometry was employed. A two dimensional point spread function (PSF) was then obtained by the optical photon distribution emitted by the screen (front side or back side). Then, the one-dimensional line spread function (LSF) along the x-axis was obtained by integrating the PSF over one axis. The MTF curve was finally calculated by performing a fast Fourier transform (FFT) of the LSF and normalizing its value to unity at zero spatial frequency (Yaffe 2000).

B.2.3.4 Swank Factor (SF) and Detective Quantum Efficiency (DQE)

The DQE of an x-ray detector characterizes the system's overall signal-to-noise transfer properties (Dick and Motz 1981a, Ranger et al 2005). These properties are related to: (a) x-ray photon absorption at different interaction depths (Nishikawa and Yaffe 1990), (b) the fluctuations in the production of the optical photons (Beutel et al

1993) and (c) the noise of the phosphor structure (grains of arbitrary size) affecting the fraction of emitted photons with respect to those produced (Nishikawa and Yaffe 1990). According to the above consideration, DQE is directly correlated with: (a) the x-ray detection efficiency η and (b) the statistical factor I, also known as Swank Factor (Swank 1974), which arises from the fluctuations in the number, m, of light photons emitted from the screen per absorbed x-ray photon. DQE was evaluated using the following formula (Dick and Motz 1981a):

$$DQE = \eta\, I \tag{7}$$

where η represents the quantum detection efficiency (see section B.2.3.1) and I is the statistical factor determined by the following equation:

$$I = \frac{M_1^2}{M_0 M_2} \tag{8}$$

where M_n is the nth moment of the light pulse height statistical distribution (statistical distribution of values of m) given as:

$$M_n = \sum_m p(m) m^n \tag{9}$$

where m is the number of light photons emitted from the screen per absorbed x-ray photon and

$p(m)$ is the (pulse height) probability distribution giving the fluctuations in the number m (optical pulse).

For a given x-ray energy the Swank factor can be expressed as the product of two separate statistical factors, I_{OPD} and I_{AED}, as follows (Swank 1974, Zhao et al 2004):

$$I = I_{OPD} I_{AED} \tag{10}$$

where I_{OPD} stands for optical pulse distribution and I_{AED} stands for absorbed energy distribution, i.e. spectrum of absorbed energy per x-ray interaction event. In the present study Poisson distribution was assumed for the production of light quanta per absorbed x-ray photon.

CHAPTER C

THE MONTE CARLO SIMULATION MODEL

The scientific method sometimes destroy alternative customs

C.1 Geometry of the simulation model

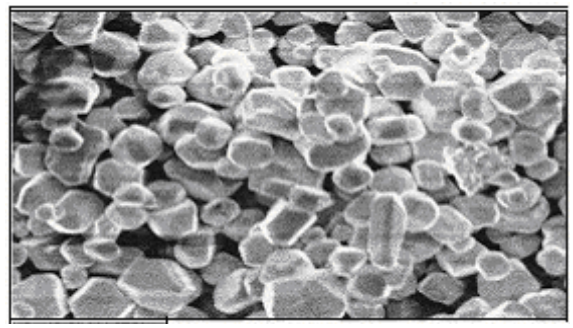

(a)

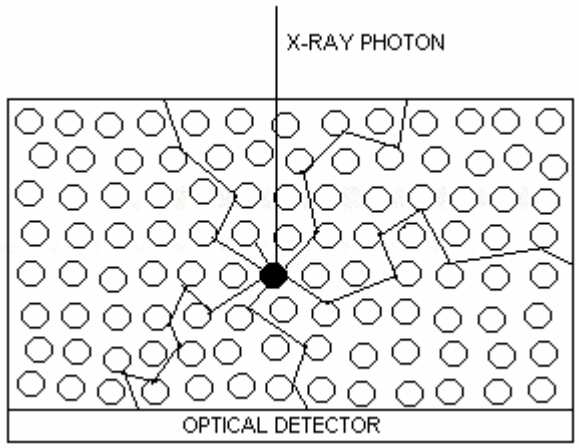

(b)

Figure 3. (a) Image of Gd_2O_2S phosphor grains, obtained by electronic microscope. (b) Schematic diagram illustrating a phosphor screen in contact with an optical detector, an x-ray photon interaction (black dot), and generated light photon trajectories (black lines).

The geometry of the simulation model is illustrated in Fig. 3. The phosphor screen was modeled as a three-dimensional layer consisting of uniformly distributed grains. All grains were of the same size, which was assumed to be equal to the mean size of the grains contained in a commercial screen (Lindstrom and Carlsson 1999). The simulation code was suitably developed in order to allow changes of the following parameters: phosphor screen (layer) thickness, screen area (surface dimensions), screen packing density and phosphor grain diameter. X-ray photons with energy either given from a monoenergetic beam or sampled from an x-ray spectral distribution, were assumed to impinge on the screen surface according to predefined beam

geometries, i.e. narrow beam or parallel beam. In addition, the role of the substrate material, between the phosphor screen and the optical detector, was taken into consideration in the validation procedure.

C.2 X-ray energy spectrum

The energy spectrum of the x-ray photons incident on the phosphor screen was sampled from data obtained via a published simulation algorithm for x-ray spectra generation (Boone and Seibert 1997, Boone et al 1997, Boone et al 1998). The x-ray spectral distribution was first normalized to generate the corresponding probability distribution function (PDF) (Morin 1988). The Monte Carlo sampling was performed by applying an inversion method (Morin 1988) to the cumulative distribution function (CDF), which was obtained by numerical integration of the PDF. Figure 4 is an illustration of a Monte Carlo spectrum distribution in comparison to a theoretical distribution of a 30 kVp x-ray Mo spectrum filtered by 0.051 mm Mo. Applying 10^6 x-ray photon histories the absolute value of the average relative difference (MC-TH)/TH between Monte Carlo (MC) and theoretical (TH) values was estimated to be 1.8%.

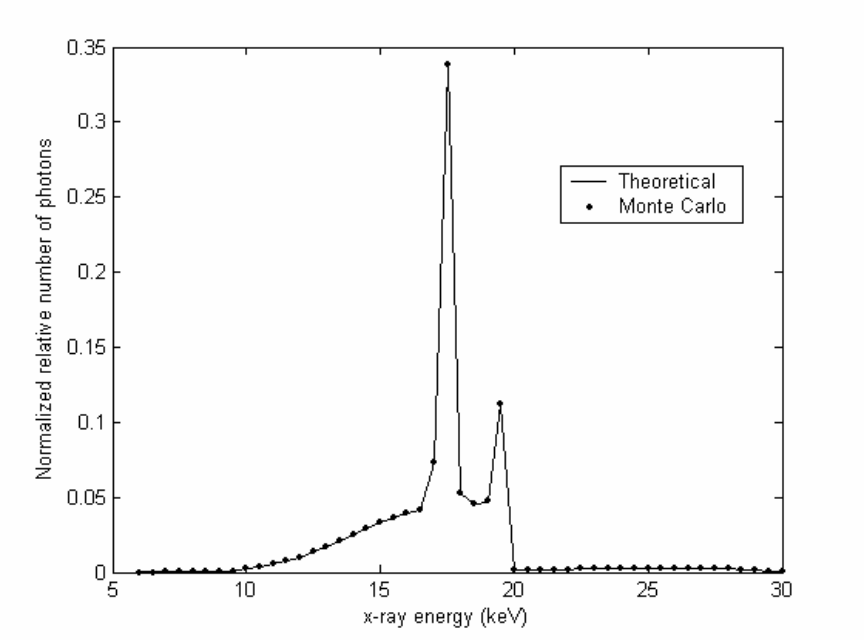

Figure 4. Comparison of Monte Carlo samples (dots) and the theoretical distribution of a 30 kVp Mo x-ray spectrum filtered by 0.051 mm Mo**.**

C.3 X-ray photon history

An x-ray photon history was considered to start when the x-ray photon, with energy obtained from the x-ray energy spectrum distribution (or from a monoenergetic beam), impinged on the phosphor screen surface. The coordinates of the initial position and the initial direction angles (polar and azimuthal) of the x-ray photon were determined according to the considered beam geometry (narrow, parallel) employing a reference coordinate system, whose origin was located at the edge of phosphor screen. For each x-ray energy value E, the total mass attenuation coefficient, the mass attenuation coefficients corresponding to each one of the x-ray interactions and the mass attenuation coefficient for each element of the phosphor were determined using logarithmic interpolation on the corresponding stored tabulated data. The x-ray photon was considered to penetrate the screen and its

transport through the phosphor slab was described in terms of the mean photon free path length (fpl) and the interaction site co-ordinates (see Appendix A).

The sampling procedure of the fpl can be verified by comparing results obtained by the Monte Carlo simulation against results obtained by the theoretical exponential probability density function, as shown in Fig. 5. Applying a monochromatic x-ray beam of 60 keV on a Gd_2O_2S: Tb phosphor screen, the average relative difference between the Monte Carlo simulation and the theoretically obtained values was 0.6%.

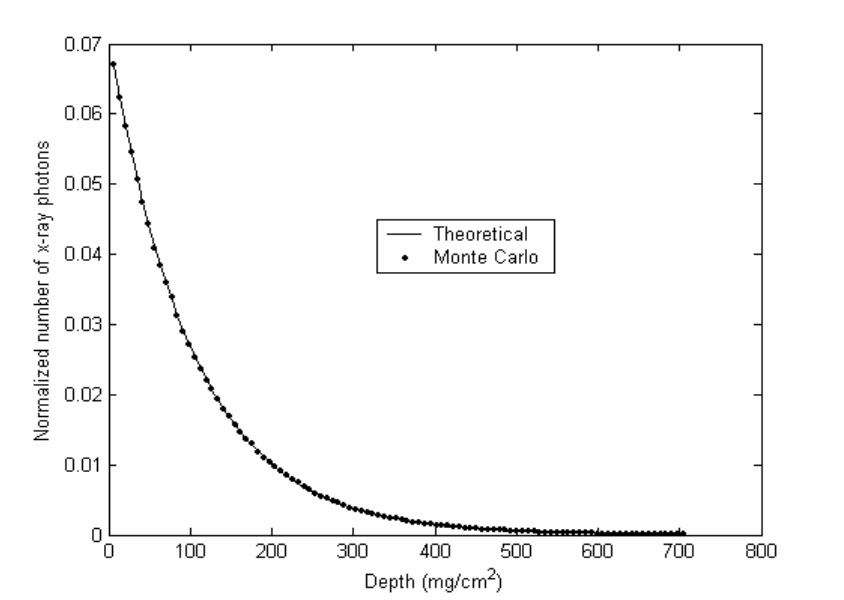

Figure 5. Comparison of 10^6 Monte Carlo samples (dots) and the theoretical curve of polar angle distribution for coherent scattering of a 60 keV monochromatic x-ray beam in Gd element.

In case of interaction, one out of three interaction processes (photoelectric effect, incoherent scattering and coherent scattering) could occur.

C.3.1 Photoelectric absorption

If the x-ray photon undergoes photoelectric absorption, a sequence of processes may occur depending on its energy E. When the photon energy is larger than the K-shell binding energy U_K, photoelectric absorption may occur either in the K-shell or in the L-shell. The probability of photoelectric absorption in the K-shell is given as:

$$P_K(E) = \frac{\sigma_{ph}^K}{\sigma_{ph}^K + \sigma_{ph}^L} \quad (11)$$

where σ_{ph}^K and σ_{ph}^L are the corresponding probabilities of K-shell and L-shell contributions to the photoelectric effect. Setting a random number R_1, photoelectric absorption occurs in K-shell if $R_1 \le P_K(E)$ otherwise it occurs in L-shell.

In the K-shell case, the emission of K-characteristic radiation or the production of Auger electrons may arise according to the K-fluorescent yield ω_K, which expresses the probability of K-characteristic radiation production in relation to the production of Auger electrons. A new random number R_2 was set such that, if $R_2 \le \omega_K$ a new x-ray photon is produced (K-characteristic photon), whose trajectory within the phosphor screen is examined separately. Otherwise, an Auger electron is emitted, which is assumed to be locally absorbed. In this study, the following K-fluorescence emission processes were considered: K-L2, K-L3, K-L-M2, K-M3, K-N2, K-N3 and K-X radiative transitions and the K-L-X Auger transitions (Sempau et al 1997), where X denotes a shell with negligible binding energy. The energy of the K-fluorescence photon or the energy deposited in the phosphor from an Auger electron was determined according to the corresponding probability of each possible transition.

The coordinates of the K-photon produced were determined from the coordinates of the interaction site of the initial x-ray photon. It was assumed that the K-characteristic photons were emitted in any direction, following an isotropic distribution. Setting two different sequences of random numbers, R_3 and R_4, the polar angle θ and the azimuthal angle ϕ were sampled according to the following cumulative density functions:

$$R_3 = P(\theta) = \int_0^{\theta} \frac{\sin\theta}{2} d\theta \;\Rightarrow\; \theta = \cos^{-1}(1 - 2R_3) \tag{12}$$

$$R_4 = P(\phi) = \int_0^{\phi} \frac{1}{2\pi} d\phi \;\Rightarrow\; \phi = 2\pi R_4 \tag{13}$$

Finally, the initial x-ray photon was assumed to be locally absorbed when: (a) the x-ray photon energy was larger than the K-shell binding energy U_K and at the same time the photoelectric effect occurred in the L-shell, (b) the x-ray photon energy was larger than the average L-shell binding energy $\bar{U}_L$ (Sempau et al 1997) and (c) the x-ray photon energy was smaller than 5 keV (cut off energy) (Morin 1988).

C.3.2 Coherent scattering

If the incident x-ray photon undergoes coherent scattering, the scattered photon acquires new direction and deposits no energy within the phosphor screen. The new direction of the scattered photon is described by the polar angle θ and the azimuthal angle ϕ, in a coordinate system that has its origin at the interaction site and its z-axis along the initial photon direction. The azimuthal angle ϕ of the scattered photon was sampled randomly in the interval $[0,2\pi)$. The polar angle θ was sampled from the differential cross section for coherent scattering, which is given by (Morin 1988, Chan and Doi 1983b):

$$\frac{d\sigma_{in}}{d\Omega} = \frac{r_e^2}{2}\left(1 + \cos^2\theta\right) F^2\left(u, Z\right) \tag{14}$$

where r_e is the classical electron radius and $F^2(u,Z)$ is the atomic form factor, which represents the probability that all the electrons of the atom take up recoil momentum without absorbing any energy. The variable u, expressed in ($Å^{-1}$),

combines the dependence of the atomic form factor on the scattering angle and on the photon energy E and is given by:

$$u = 29.1433\left(\frac{E}{m_0 c^2}\right)(1-\cos\theta)^{1/2} \tag{15}$$

where $m_o c^2$ is the rest mass energy of an electron. The polar angle θ was sampled from the differential cross section for coherent scattering using the sampling algorithm described by Chan and Doi (1983b) (see Appendix B). The sampling procedure was verified by comparing results obtained by Monte Carlo simulation with the theoretical polar angular distribution (equation (4) scaled by $\frac{1}{r_e^2}$), as shown in Fig. 6. The average relative difference between Monte Carlo and theoretical values was found 2.4%.

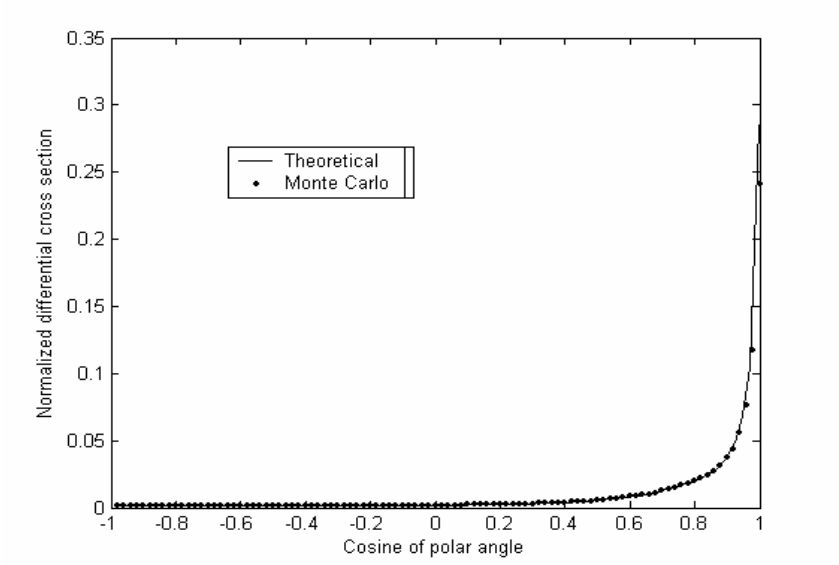

Figure 6. Comparison of 10^6 Monte Carlo samples (dots) and the theoretical curve of polar angle distribution for coherent scattering of a 60 keV monochromatic x-ray beam in Gd element.

C.3.3 Incoherent scattering

If the incident x-ray photon undergoes incoherent (Compton) scattering through collision with a loosely bound atomic electron, it transfers some of its energy and

momentum to the electron (recoil electron) and it is deflected an angle θ with respect to its original direction. The energy E_C of the scattered photon is given by:

$$E_C = \frac{m_0 c^2 E}{m_0 c^2 + E(1-\cos\theta)} \tag{16}$$

where E is the energy of the incident photon. The difference $E - E_C$ goes to the recoil electron as kinetic energy, assuming that the electron had negligible binding energy. The differential cross section of incoherent scattering, including electron binding effects, is given by:

$$\frac{d\sigma_{in}}{d\Omega} = \frac{r_e^2}{2}\left(\frac{E_C}{E}\right)^2\left(\frac{E_C}{E} + \frac{E}{E_C} - \sin^2\theta\right)S(E,\theta) \tag{17}$$

where $S(E,\theta)$ is the incoherent scattering function of an atom, which represents the probability that an atom will be raised to any excited or ionized state, when a photon imparts a recoil momentum to an atomic electron. The recoil electron was assumed to be locally absorbed and the scattered photon was assumed to be transported within phosphor material having a new direction and energy. The new direction of the scattered photon is described by the polar angle θ and the azimuthal angle ϕ, in a coordinate system that has its origin at the interaction site and its z-axis along the initial photon direction. The azimuthal angle ϕ of the scattered photon was sampled randomly in the interval $[0,2\pi)$. The polar angle θ was sampled from the differential cross section for incoherent scattering, using the sampling algorithm described by Brusa et al (1996) (see Appendix C).

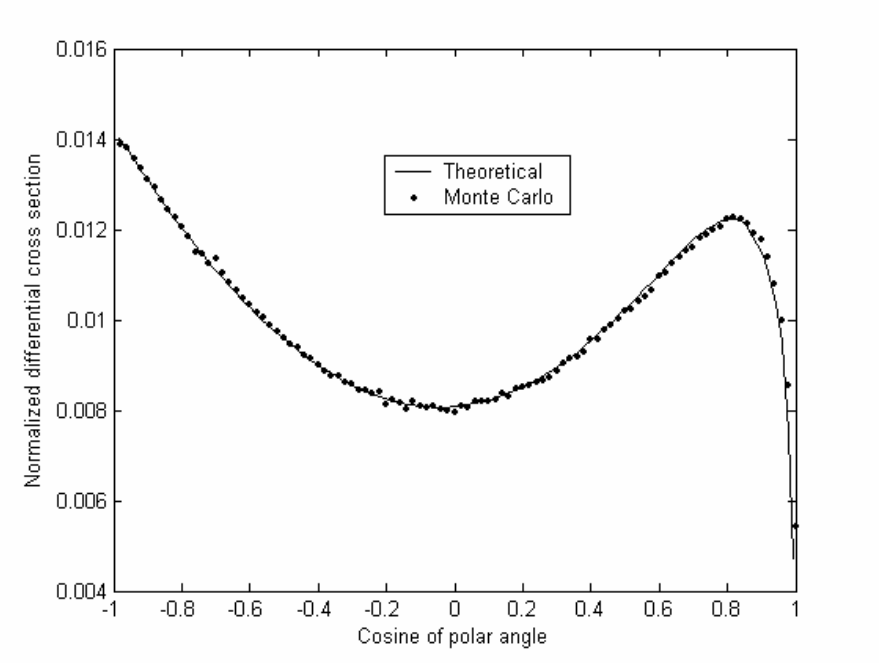

Figure 7. Comparison of 10^6 Monte Carlo samples (dots) and the theoretical curve of polar angle distribution for incoherent scattering of a 60 keV monochromatic x-ray beam in Gd element.

The sampling procedure was verified by comparing results obtained by Monte Carlo simulation with the theoretical polar angular distribution, as shown in Fig. 7. The average relative difference between Monte Carlo and theoretical values was found 2.1%.

C.4 Light production

After an x-ray interaction event, contributing to energy deposition within the phosphor material, light photons are created following an isotropic distribution. The number G of these light photons is given as follows (Nishikawa and Yaffe 1990):

$$\overline{G}(E) = \eta_C \frac{E}{\overline{E}_\lambda} \tag{18}$$

where E is the absorbed energy of the x-ray photon, η_c is the intrinsic x-ray to light conversion efficiency (Blasse 1994) of the phosphor, and $\overline{E_\lambda}$ is the mean energy of

the light photons created within the phosphor mass. Mean energy was employed in relation (1) instead of the whole light spectrum. We used the value $E_{\lambda} = 2.4 \times 10^{-3}\ keV$, which corresponds to the mean light photon energy of the Gd_2O_2S: Tb phosphor (Nishikawa and Yaffe 1990). The simulation of the light spectrum is quite complicated, because of the statistical uncertainties arising from: (a) the electron transition probabilities in the low energy atomic levels (Sempau 1997) and (b) the effects of the activator on these levels (Blasse 1994, Morlotti et al 1997). It has been previously shown that the statistical fluctuations of the x-ray to light conversion process follow a probability distribution, which has not_been expressed analytically. However, it may be approximated using experimental data (Beutel et al 1993, Beutel and Kittis 1996). The excess of this distribution function over a Poisson distribution has been expressed (Beutel et al 1993, Beutel and Kittis 1996) by the Poisson excess noise (ε) given as follows:

$$\varepsilon = \left(\frac{\sigma^2_{G(E)}}{\overline{G}(E)} \right) - 1 \tag{19}$$

where $\overline{G}(E)$ is the average number of light photons produced per absorbed x-ray photon and $\sigma^2_{G(E)}$ is the variance of the probability distribution. In the present study, the Swank factor (Swank 1974) as well as the DQE values were predicted by sampling the number of produced light photons, using the particular probability distribution, and by determining the corresponding statistical moments (m_i) of the light distribution detected by the optical detector (Dick and Motz 1981a, Dick and Motz 1981b, Ginzburg and Dick 1993).

C.5 Light transport

Just after their creation, light photons are transmitted through the screen material towards the screen surfaces. During transmission, light suffers attenuation mainly, caused by the presence of the phosphor grains. Since the geometry of our model implies a homogeneous distribution of phosphor grains, Mie theory (Van de Hulst 1957) can be applied to describe adequately the light extinction within a phosphor screen (see Appendix D). At the site of light photon interaction, the type of interaction may be determined by the relative probabilities of light absorption and light scattering effects. The probability of light absorption P_{abs} is defined as follows:

$$P_{abs} = m_{abs} / (m_{abs} + m_{sct}) \quad (20)$$

where m_{abs}, m_{sct} correspond to light absorption and light scattering coefficients, respectively. The azimuthal angle ϕ of the scattered photon was sampled randomly in $[0,2\pi)$. The polar angle θ was sampled from the Henyey-Greenstein (Peters et al 1990, Graaff et al 1993) (see Appendix E) probability density function, which is a good approximation of the phase function for light photons scattered according to Mie theory. The sampling procedure can be verified by comparing results obtained by Monte Carlo simulation with the theoretical polar angular distribution, as shown in Fig. 8. Assuming grain diameter equal to 7 μm for Gd_2O_2S:Tb phosphor material (anisotropy factor $g = 0.494$, see Appendix E), the average relative difference between Monte Carlo and theoretical values was found 1.2%. As described above, light propagation was simulated via Mie theory. Applying Mie calculations, light absorption and light scattering coefficients, m_{abs}, m_{sct}, are related to the absorption, Q_{abs}, and the scattering, Q_{sct}, efficiency factors (Bohren and Huffman 1983, Van de

Hulst 1957, Hong Du 2004) and to the complex elements, $S_1(\theta)$ and $S_2(\theta)$, of the scattering matrix (Bohren and Huffman 1983, Van de Hulst 1957, Hong Du 2004).

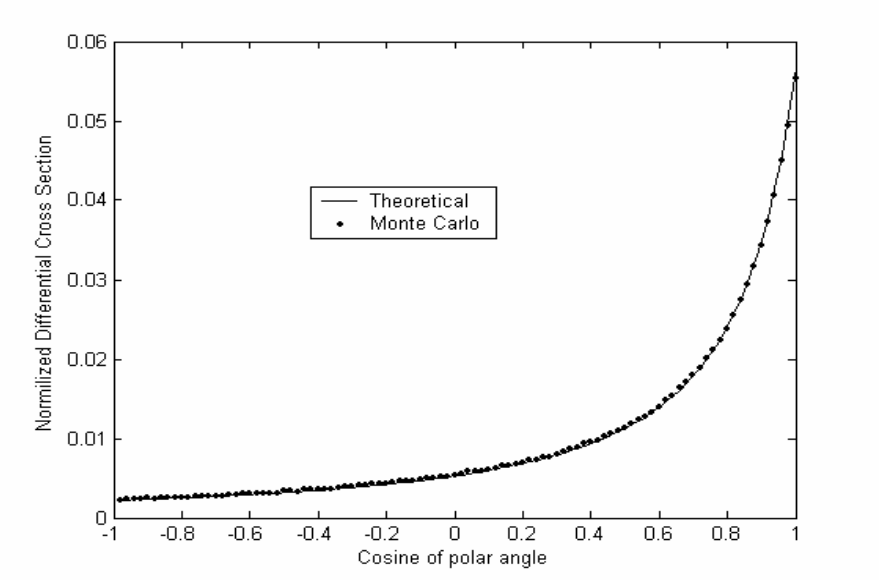

Figure 8. Comparison of 10^6 Monte Carlo samples (dots) and the Henyey-Greenstein theoretical distribution of polar angle distribution for Gd_2O_2S:Tb phosphor screen with grain size 7 μm.

These quantities were correctly simulated according to the validation that is shown in table I (see Appendix D). The comparison was carried out for data relative to the numerical values, which correspond to the complex refractive index of phosphor materials (complex refractive index of Gd_2O_2S:Tb: $2.3\text{-}10^{-6}i$, where 2.3 and 10^{-6} represent the real and the imaginary parts, respectively). For the Gd_2O_2S:Tb phosphor material, Moy(2000) has reported a refractive index value of higher than 2. Radcliffe et al (1993) have used a value of 2.4 in combination with a value of 1.4 for the refractive index of the binder, both of which gave a reasonable fit to experimental data. In the present study, the real part of the complex refractive index of Gd2O2s:Tb was taken equal to 2.3 using binder's refractive index (Giakoumakis 1990) equal to 1.353. Following previous studies (Morlotti 1975, Bohren and Huffman 1983), the imaginary part was assumed to be of the order of 10^{-6}, for wavelengths within the visible region.

Table I. Comparison of Q_{ext}, Q_{sca}, $S_1(0)$, $S_2(0)$, $S_1(\pi)$ and $S_2(\pi)$ between Hong Du (2004) calculations and these obtained from our study.

	M	X	Q_{ext}	Q_{sca}	$S_1(0)=S_2(0)$	$S_1(\pi)=-S_2(\pi)$
Present study	$1.33\text{-}10^{-5}$i	100	2.10132	2.09659	5253-24.319i	-56.5921+484.251i
Hong Du (2004)	$1.33\text{-}10^{-5}$i	100	2.10132	2.09659	5253-24.319i	-56.5921+484.251i

C.6 Reflection at the boundaries

During a light photon trajectory, when the light photon hits one of the phosphor screen boundaries, it may either escape or internally be reflected. If we consider that z_0 and z_1 are the corresponding z coordinates of the front and rear side boundaries of phosphor screen, the trajectory of light photon may be indicated according to the following procedure:

(i) The distance d_1 between the last light photon interaction site and the boundary is calculated:

$$d_1 = \begin{cases} (z - z_0)/(-\cos\theta), & for\ \cos\theta < 0 \\ (z_1 - z)/\cos\theta, & for\ \cos\theta > 0 \end{cases} \quad (21)$$

(ii) The angle of incidence θ is evaluated and, with the help of Snell's law, the angle of transmission ω is calculated as a function of θ, of the relative complex refractive index of the phosphor screen m_i (phosphor material) and of the refractive index of the transmitting medium m_t (air, film or photosensitive material), as follows:

$$\theta = \cos^{-1}\left(|\cos\theta|\right) \text{ and } \omega = \sin^{-1}\left(\frac{m_i}{m_t}\sin\theta\right) \quad (22)$$

(iii) The probability of the average light photon specular reflectance can be calculated from Fresnel's formulas (Bohren and Huffman 1983, Giakoumakis and Nomicos

1985) multiplied by a factor S_C correcting for the roughness of the screen's surface, given by the following equation (Giakoumakis and Nomicos 1985, Roos and Ronnow 1994):

$$S_C = \exp\left[-\left(\frac{2\sqrt{2}\pi n\delta}{\lambda}\right)^2\right] \tag{23}$$

where δ is the root mean square (rms) roughness expressing surface irregularities, λ is the light wavelength, and n is the real part of the refractive index of the transmitting medium. Values of S_C near to unity imply interfaces of high surface smoothness. For example, assuming $\delta = 3\,mm$, $n = 1.5$ and $\lambda = 545\,nm$, equation (6) results in a factor S_C equal to 0.988, implying a slight reduction in specular reflectance. Therefore, surface irregularities may cause: (a) a slight reduction in specular reflectance and (b) the presence of diffuse reflectance. In the latter case, light photons are reflected in random directions. In the present study, light specular reflectance was simulated assuming smooth boundary surface and, thus, the effect of diffuse reflectance was not taken into consideration.

(iv) The light photon is internally reflected, otherwise it escapes the phosphor screen. In case of reflection, the light photon transportation is described as follows (Wang et al 1995):

(a) a new direction is calculated by transforming the direction cosines to $(a,b,c) = (\sin\theta\cos\phi, \sin\theta\sin\phi, -\cos\theta)$

(b) the light photon propagates within phosphor material having a new free path length equal to $fpl - d_1$.

C.7 Required input data to the Monte Carlo program

The input physical data, required for the Monte Carlo simulation program, included the phosphor material's chemical composition, the x-ray photon's spectral distribution and the numerical values of various physical parameters and coefficients relevant to x-ray interactions and to optical properties of the material. All values were taken from validated tabulated data and libraries. In particular, the parameters and coefficients employed were the following:

Data relevant to the x-ray spectrum (Boone and Seibert 1997, Boone et al 1997, Boone et al 1998), the mass attenuation coefficients of the material (Berger et al 1999, Zaidi 2000, Boone and Chavez 1996), the mass partial interaction coefficients of the material (Berger et al 1999, Zaidi 2000, Boone and Chavez 1996), the mass partial interaction coefficients of each element of the chemical compound and their fractional weight (Berger et al 1999, Zaidi 2000, Boone and Chavez 1996), the incoherent scattering functions (Hubbell et al 1975), the atomic form factors (Hubbell et al 1975), the probability of the K or L-shell contribution to the photoelectric effect (Zaidi 2000, Boone and Chavez 1996, Cullen et al 1997), the K-fluorescent yield (Hubell et al 1994) for the production of characteristic radiation or the probability of Auger electron production, the K or L shell binding energies (Cullen et al 1997), the transition probabilities of atom relaxation (Cullen et al 1997), the refractive index of the phosphor material (Radcliffe et al 1993, Moy 2000) and of the medium (Giakoumakis et al 1990), the phosphor's intrinsic conversion efficiency (Yaffe 2000) and the wavelength of the emitted light (Yaffe 2000).

C.8 Output parameters

Employing the previously described simulation, numerical evaluations concerning the x-ray and light photon absorption or escape events were carried out. Additionally, for every x-ray interaction and absorption event, information on the deposited amount of the x-ray energy, as well information on the spatial distribution of the emitted light was obtained. These evaluations and the corresponding information were used in the evaluation of the following phosphor screen parameters and imaging characteristics:

(i) The Quantum Detection Efficiency (QDE) corresponding to the number of absorbed *x*-ray photons with respect to the incident x-ray photons.

(ii) Energy Absorption Efficiency (EAE) corresponding to the absorbed energy of primary radiation with respect to the incident x-ray energy.

(iii) The number of emitted light photons per incident x-ray photon.

(iv) The Point Spread Function (PSF): The two-dimensional spatial position of light photons along screen length.

(v) The Modulation Transfer Function (MTF): The Discrete Fourier Transform (DFT) of the line-spread function (LSF), which was obtained by integrating the PSF over one axis.

(vi) The Detective Quantum Efficiency (DQE) expressed by the Swank Factor (SF) multiplied by the Quantum Detection Efficiency (QDE). The Swank Factor was obtained by evaluating the corresponding statistical moments (m_i) of the light distribution detected by the optical detector.

Applying 10^4 monoenergetic x-ray photons of 18 keV ($9 \cdot 10^6$ light photon histories) for Gd_2O_2S:Tb phosphor material (thickness: 31.7 mg/cm^2, grain size: 7 μm, packing

density: 50%), approximately 14 hours of computation time is required using a single-processor P4 with 3.00 GHz and 512 Mbyte access memory.

CHAPTER D

VALIDATION, RESULTS AND DISCUSSION

The truth of a particular proposition cannot be evaluated with respect to an "absolute truth"

D.1 Validation and Results

Monte Carlo techniques are used in medical physics applications to simulate the physical phenomena (radiation and light interactions) that take place within the material under investigation. Each sampling procedure that produces a physical parameter has to be validated by comparing the obtained distribution with the theoretical one. All distributions produced in the present study were validated as shown in the description of the Monte Carlo model (see Section C). However, the validity of Monte Carlo models has to be verified by comparing data obtained by the Monte Carlo simulation with experimental data associated to macroscopic measurements.

D.1.1 Validation-The QDE and EAE metrics

The quantum detection efficiency of Gd_2O_2S: Tb phosphor with respect to the incident x-ray energy is shown in figure 9. In this figure Monte Carlo results are compared with experimental data obtained by Dick and Motz (1981), for energies ranging from 18 keV to 69 keV. The curves correspond to 31.7 mg/cm^2 screen coating weight, 7 μm mean grain size with 50% packing density (Blasse and Gramaier 1994, Nishikawa and Yaffe 1990). QDE was evaluated, by considering parallel, 3 mm thick, monoenergetic x-ray beams. In this evaluation, the number of re-absorbed K x-ray photons for energies above the K-edge of the Gd element, was also taken into account. All curves correspond to data obtained behind the non-irradiated screen surface. This configuration is often referred to as front screen configuration or transmission mode and corresponds to the screen-optical detector combination incorporated in digital imaging detectors. Results for the energy absorption efficiency

(EAE), obtained under similar conditions, are also given in the same graph. Both QDE and EAE were estimated with a statistical error less than 0.1%.

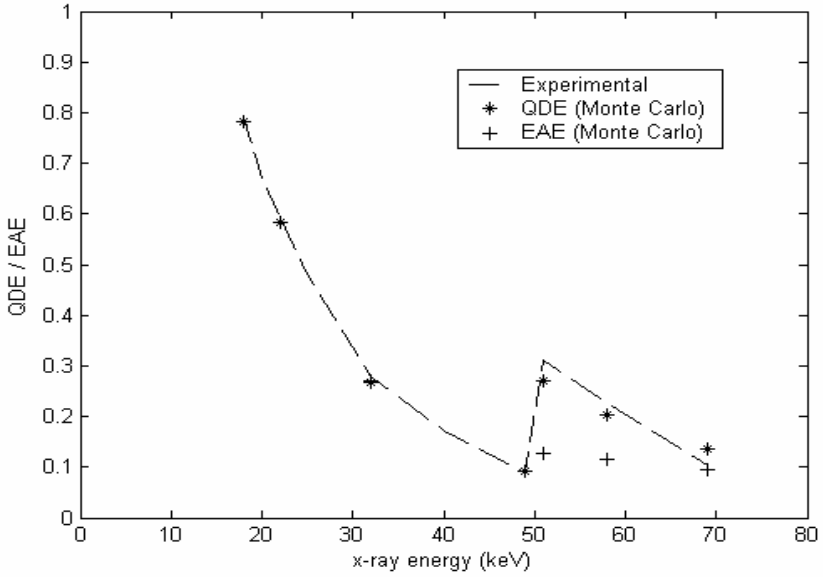

Figure 9. The variation of QDE and EAE as a function of the incident x-ray energy. Comparison between Monte Carlo values (dots) and experimental (QDE) measurements (Dick and Motz 1981)for Gd_2O_2S:Tb phosphor material (thickness: 31.7 mg/cm^2, packing density: 50%, grain size: 7 μm).

QDE and EAE were found almost identical in the energy range from 18 keV to 25 keV. Above 25 keV, the values of EAE were found slightly higher than QDE. This difference was due to the increasing number of scattering events (inelastic scattering) occurring for energies higher than 25 keV. Even if scattered photons escape the screen, and thus not accounted for in the calculation of QDE, a small fraction of energy is still deposited within the phosphor. This small fraction increases slightly the values of EAE with respect to those of QDE. Above 50.2 keV, a K-fluorescence photon is generated that may escape the phosphor screen, even though the incident x-ray photon is totally absorbed. The energy conveyed by the K-fluorescence photon is considerably higher than the energy locally deposited by the incident photon. As a result, QDE values, expressing the fraction of absorbed incident x-ray photons, are

significantly higher than those of EAE, expressing the fraction of locally absorbed energy.

D.1.2 Validation-The light emitted per absorbed x-ray

Table II shows the number of light photons emitted by the non-irradiated screen surface (transmission mode or front screen configuration) per absorbed x-ray photon for various x-ray photon energies from 18 keV to 69 keV. Monte Carlo results are compared with experimental data from the work by Dick and Motz (1981). These data were obtained under experimental irradiation conditions similar to those simulated in our method. In the evaluation of light photons per absorbed x-ray photon, the light reflection at the screen-substrate (Ludwig and Prener 1972) interface was also taken into account (see section C.6). The average value of light reflectance $R(\theta)$, for all possible incident angles at the screen-substrate interface, was found approximately equal to 0.30 (fraction of escaped light photons 70%). This value was obtained using the following data for the relative complex refractive index: $m_{material} = n_{grain} / n_{medium} = 2.3/1.353 = 1.7$ and $m_t = 1.52$, where $m_{material}$ is the relative complex refractive index of the phosphor screen (m_i in equation (22)), n_{grain} is the reflective index of the phosphor material (Gd_2O_2S:Tb), n_{medium} is the reflective index of the binder material (Na_2SiO_3) (Giakoumakis et al 1990) and m_t is the refractive index of the transmitting medium m_t (glass).

Table II. Comparison of the number of emitted light photons per absorbed x-ray between Dick and Motz (1981) experimental measurements and those obtained in our study for various incident x-ray energies.

	Gd_2O_2S:Tb (thickness 31.7 mg/cm^2)						
Incident energy (keV)	18	22	32	49	51	58	69
	Number of emitted light photons per absorbed x-ray						
Dick and Motz (1981)	365 ± 73	470 ± 94	645 ± 129	945 ± 189	700 ± 140	785 ± 157	890 ± 178
Present study	356 ± 3	463 ± 4	695 ± 12	1089 ± 43	710 ± 8	924 ± 25	1282 ± 37

Apart from the data obtained at 69 keV, our Monte Carlo simulation results are in adequate agreement with the results from experimental measurements. Deviations from full coincidence may be reasonable if we consider: (a) the estimated uncertainty in experimental data (Dick and Motz 1981), which is of the order of 20%, (b) the possible count loss during experimental measurements(Dick and Motz 1981), which is 3%, (c) the error, in our model, arising from the assumption of monochromatic light photons (Nishikawa and Yaffe 1990), (d) the statistical error in coefficients taken from data bases (Zaidi 2000, Boone and Chavez 1996), (e) the systematic error arising from our assumption of 50% packing density, 7 μm grain size and 0.15 intrinsic efficiency and (f) the statistical error that arise from Monte Carlo simulations.

D.1.3 Validation-The MTF metric

Figure 10 illustrates a comparison between an experimentally determined (Nishikawa and Yaffe 1990) and a Monte Carlo simulated modulation transfer function (MTF) of a Gd_2O_2S:Tb screen (thickness: 31.7 mg/cm^2, grain size: 7 μm, packing density: 50%). Both curves correspond to similar irradiation conditions: 30 kVp poly-energetic molybdenum x-ray spectrum, filtered by 0.051 mm of molybdenum and 4.2 cm of Lucite to simulate beam hardening by an average breast.

Additionally, narrow beam geometry at the centre of phosphor screen surface was assumed (Nishikawa and Yaffe 1990). As it can be observed in Fig. 10, there is a high degree of coincidence between the experimental and the Monte Carlo predicted MTF values. In fact, it was calculated that the absolute value of the average relative difference between the two curves at all spatial frequencies was 1%.

The latter resulted from the slightly higher Monte Carlo simulated values. This systematic error may probably have arisen from our assumption of constant grain size (equal to the alleged by the manufacturer (7 μm)). If this is not the case, then a deviation from the experimental MTF may be expected, due to variations in packing density (or grain spatial distribution) and in grain size. In the present study, the MTF of the film was taken to be unity (Beutel et al 1993, Bunch et al 1987).

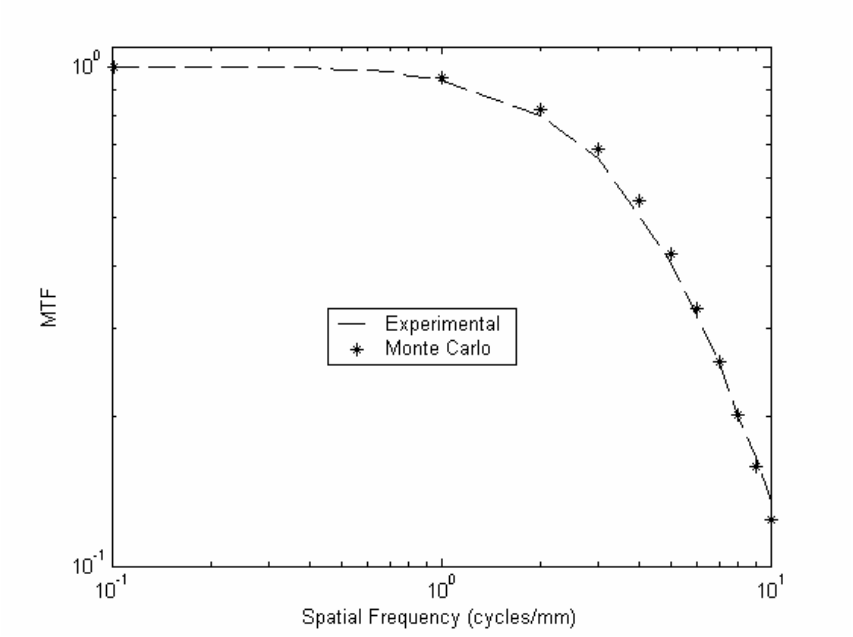

Figure 10. The variation of MTF as function of spatial frequency. Comparison between Monte Carlo values (dots) and experimental measurements (Nishikawa and Yaffe 1990) for Gd_2O_2S:Tb phosphor material (thickness: 31.7 mg/cm^2, packing density: 50%, grain size: 7μm, x-ray tube voltage: 30 kVp, filter: 0.0051 mm Mo, 4.2 cm Lucite).

D.1.4 Validation-The zero frequency DQE metric

Table III gives the DQE values with respect to x-ray energy. Monte Carlo values are compared with experimental data, obtained by Dick and Motz (1981) for energies ranging from 18 keV to 69 keV. Up to the energy of K-absorption edge, DQE values were estimated assuming a Poisson distribution. (i.e. $\varepsilon = 0$, see equation (19)). For x-ray energies above the K-edge, DQE values were predicted by: (a) taking into account the QDE values obtained by the detected incident x-ray photons (Dick and Motz 1981a, Dick and Motz 1981b, Ginzburg and Dick 1993) and (b) evaluating the Swank factor, assuming a Poisson distribution at 51 keV and 58 keV, and a non-Poisson distribution at 69 keV, considering $\varepsilon / \overline{G}(E) = 0.3$ (see equation 19). DQE values were found to be in excellent agreement with the experimental data.

Table III. Comparison of DQE values between Dick and Motz (1981) experimental measurements and those obtained in our study for various incident x-ray energies.

	Gd_2O_2S:Tb Phosphor thickness:31.7 mg/cm^2						
Incident energy (keV)	18	22	32	49	51	58	69
	Detective quantum efficiency (DQE)						
Dick and Motz (1981)	0.58	0.44	0.19	0.07	0.18	0.14	0.07
Present study	0.57	0.43	0.20	0.07	0.16	0.14	0.07

D.1.5 The contribution of physical processes to light production

Table IV shows data obtained by the Monte Carlo model corresponding to the fraction of emitted light (in transmission mode) with respect to the light produced within the phosphor, as well as with respect to the contribution of various energy deposition processes to the emitted light. The energy deposition processes considered, were the following: (a) x-ray photons absorption without undergoing any scatter

event, (b) x-ray photons absorption, after, at least, one scatter event, (c) K-characteristic photons absorption, (d) energy deposition by Auger electrons produced in the K-shell, and (e) energy deposition by electrons released during inelastic scattering. All data provided correspond to Gd_2O_2S:Tb phosphor (thickness: 31 mg/cm^2, grain size: 7 μm, packing density: 50%), in the energy range from 18 keV up to 69 keV.

Table IV. Light emitted per light produced of Gd_2O_2S:Tb (thickness 31.7 mg/cm^2) for various incident x-ray energies. Contribution of each physical process to the emitted light (transmission mode).

	Gd_2O_2S:Tb (thickness 31.7 mg/cm^2)			
Incident energy (keV)	18	49	51	69
Light emitted per light produced % (Front screen)	42.41 ± 0.16	48.64 ± 0.69	47.35 ± 0.29	47.94 ± 0.43
	Contribution to light emitted (Front screen configuration)			
Local deposition of the initial photon % (without scatter event)	97.46 ± 0.19	97.82 ± 0.5	62.82 ± 1.01	78.26 ± 0.62
Local deposition of the initial photon % (with scatter event)	2.53 ± 0.19	1.83 ± 0.48	0.81 ± 0.23	0.78 ± 0.16
K-Characteristic radiation %			25.96 ± 0.46	14.91 ± 1.02
K-Auger electrons %			10.26 ± 0.74	5.67 ± 0.64
Compton electrons %	0.0057 ± 0.0022	0.34 ± 0.08	0.15 ± 0.02	0.36 ± 0.05

D.1.6 The effect of grain size and packing density on MTF

To investigate the effect of grain size and packing density on MTF, Monte Carlo results, shown in Figs 11 and 12, were obtained. As it can be observed, both grain size and packing density affect significantly MTF values. Higher MTF corresponds to small grain size (Fig. 11) and high packing density (Fig. 12). The effect of grain size

and packing density may be explained by considering that the increased number of grains, either in a small sized grain distribution or in a denser distribution, increases the number of light scattering events. In that case, laterally directed light photons, which follow large distances to escape the screen, undergo a larger number of interactions. Therefore, the probability of lateral photon extinction increases. Thus, the total amount of light propagates to the screen output following a spatial distribution of higher forward directivity, resulting in better MTF values (Giakoumakis et al 1980).

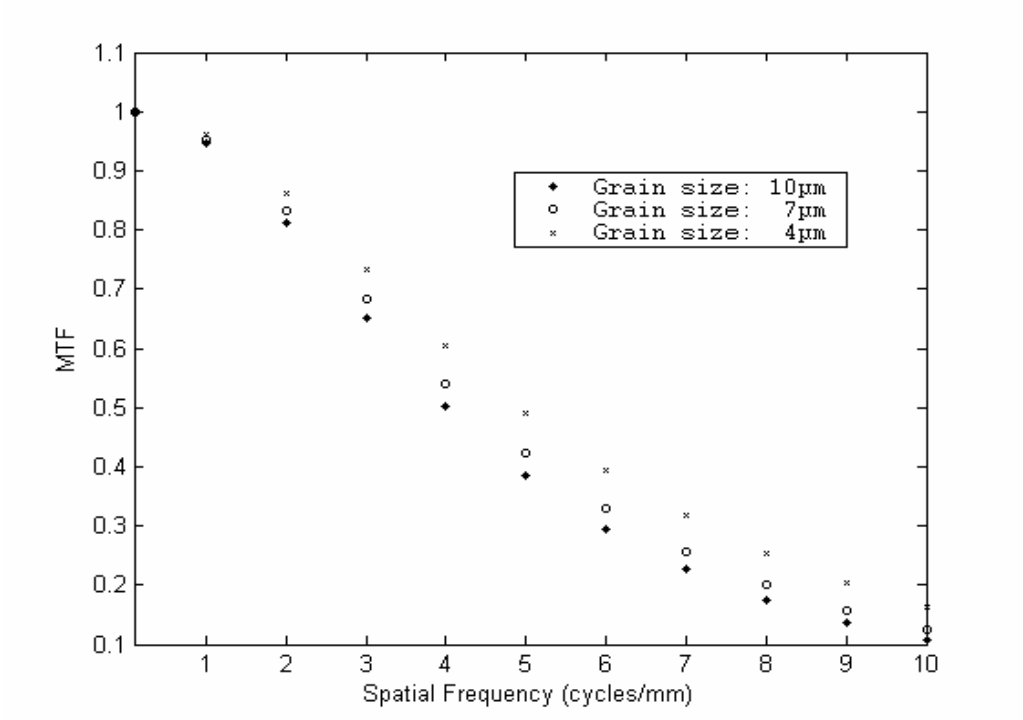

Figure 11. The variation of MTF as function of spatial frequency for three different grain sizes (4 μm, 7 μm, 10 μm) for Gd_2O_2S:Tb phosphor material (thickness: 31.7 mg/cm^2, packing density: 50%, x-ray tube voltage: 30 kVp, filter: 0.0051 mm Mo, 4.2 cm Lucite).

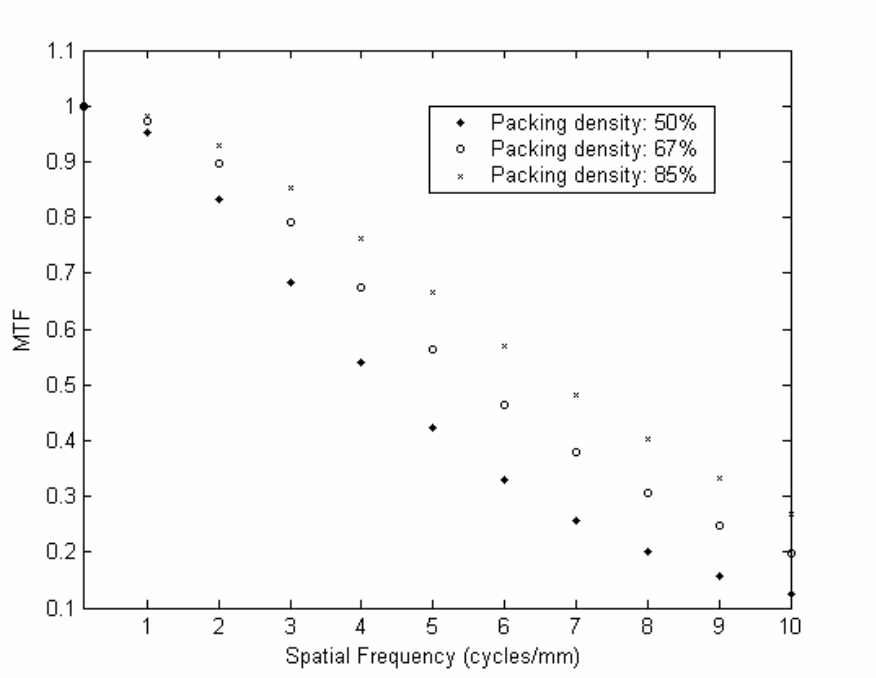

Figure 12. The variation of MTF as function of spatial frequency for three different values of packing density (50%, 67%, 85%) for Gd_2O_2S:Tb phosphor material (thickness: 31.7 mg/cm^2, grain size: 7 μm, x-ray tube voltage: 30 kVp, filter: 0.0051 mm Mo, 4.2 cm Lucite).

D.2 Discussion

The light interactions within phosphor materials has been previously described in terms of optical parameters incorporated in analytical models published by Hamaker, Ludwig, and Swank (Hamaker 1947, Ludwig 1971, Ludwig and Prener 1972, Swank 1974). These models have been developed either by assuming one-dimensional light propagation, or by using suitable approximations to the photon diffusion equation. The values of the optical parameters have been obtained by fitting model equations to experimental data. However, it has been observed that these values were, more or less, affected by the thickness of the phosphor. This was attributed to the limitations of the aforementioned models to accurately express phosphor inhomogeneities arising from the granular structure of the screens. The optical coefficients related to these models have been also used in Monte Carlo studies (Morlotti 1975) to simulate light interactions within phosphor screens. Badano et al.(2004) developed a model using

the DETECT II simulation code and provided a better fit to experimental data. In the present study, the material's complex refractive index was used as an input optical parameter. Following previous studies (Morlotti 1975, Bohren and Huffman 1983, Van de Hulst 1957, Hong Du 2004), it was considered that in a phosphor material the real part of the refractive index indicates light scattering, and the imaginary part indicates light absorption. It was also assumed that the imaginary part of the material's complex refractive index is not negligible. Using refractive index data and applying Mie scattering theory in our calculations, microscopic probabilities were used to simulate light transport within the phosphor material. Based on such considerations, we have developed our model in such a way that, apart from the complex refractive index, the only optical data required to express screen properties and their effect on image characteristics were the values of the intrinsic conversion efficiency and the light wavelength. Within this treatment, the relative probability of light absorption, with respect to light scattering, depends on the size of phosphor grains and on the wavelength of the transmitted light. At the phosphor screen output, the fraction of escaping light photons was related to the number of light interaction events taking place within the phosphor material. For a given grain size and packing density, this number was also associated to the corresponding phosphor screen thickness. It has been previously estimated that analytical models, based on diffusion equation, can not accurately describe the performance of thin screens and corresponding results are of limited accuracy (Giakoumakis et al 1991). The present study attempts to overcome these limitations. The light spatial distribution at screen output can be predicted and information of phosphor screen performance for different virtual experimental setups can be extracted.

As it may be observed from Fig. 9, the values predicted for the QDE, show slight deviations with respect to experimental data. These deviations appear more clearly at energies above the K-edge. At these energies, both experimental data and our Monte Carlo results are affected by the presence of the K-characteristic radiation. In order to investigate this effect, the simulation of K-characteristic radiation was examined by comparing the fraction of escaped K-photons, as predicted by our code, with previous calculations (Venema 1979).

Table V. Comparison of the escaped K-photons fraction between Venema (1979) calculations and these obtained from our study.

	Gd_2O_2S:Tb (thickness 105 mg/cm^2)		
Incident energy (keV)	51	58	69
	Fraction of escaped K-photons		
Present study	60.45% ± 0.24	60.52% ± 0.25	60.21% ± 0.29
Venema (1979)	60%		

As it is shown in table V, both data were found to be in excellent agreement. Hence, the deviations may be probably due either to experimental uncertainties or to uncertainties in the attenuation coefficients values above the K-edge of published data (Berger et al 1999). In addition, attenuation coefficient uncertainties, which have been also discussed by Chan and Doi (1983b), may also be responsible for deviations in the prediction of emitted light photons per absorbed x-ray, especially at 69 keV (see table II).

To further investigate this issue, e.g. the influence of the x-ray coefficient uncertainties on the accurate determination of the emitted light, we tried to show that light is attenuated in the same manner independently from the input value of the incident x-ray energy (e.g. 51 keV, 58 keV, 69 keV). In this case, we may expect equal portions of the generated light photons to escape the phosphor (from the both

sides: irradiated and non-irradiated) for different values of incident x-ray energy. This would imply that the total number of the emitted light photons, or the total light energy fluence emitted by the screen, is proportional to the number of the light photons generated within the phosphor, which in turn is proportional to the total amount of x-ray energy deposited. Hence, in order to test the aforementioned consideration, the ratio of the total light energy fluence emitted by both screen surfaces (both the irradiated and the non-irradiated sides) over the total amount of energy absorbed, was examined. This ratio was evaluated for various incident x-ray photon energies. More specifically, by applying x-ray beams with corresponding energies 51 keV, 58 keV and 69 keV, the above ratio was found equal to 0.1492. This invariable value of the ratio, which equals to the intrinsic efficiency ($n_c = 0.15$) minus the fraction of light energy flux absorbed in the phosphor, indicates that light losses are similar for all x-ray energy values. Therefore, variations in the amount of the emitted light in each phosphor screen side are due to the absorbed energy depth distribution at the corresponding incident x-ray energy. Taking into account that for each 1 keV x-ray energy deposition, 62 light photons are produced, small deviations in the energy depth of the absorbed x-rays could cause quite big deviations in the amount of light emitted by each screen surface. Actually, according to Nishikawa and Yaffe model (Nishikawa and Yaffe), for phosphor screens of equal thickness, each variation on the amount of light that escapes to the screen output is due to the depth of each x-ray interaction and the corresponding amount of the deposited energy on it. According to MTF data shown in figures 11 and 12, the size of the phosphor grains and their spatial distribution (packing density) affect significantly the MTF values, which improve with decreasing grain size and with increasing packing density. It has been previously shown that screen packing density may remain invariant when the

size of the grains varies (Lindstrom and Carlsson 1999). However, Blasse and Grabmaier (1994) suggested that apart from obtaining the desired particle size, powder materials with a reduced porosity (higher packing density) can be synthesized. This may be achieved using a sintering process at elevated temperature to produce phosphor layers in ceramic form. In such a case, the increased fraction of grains within phosphor screen increases the number of light scattering events. Under Mie scattering conditions, this increases the overall directivity of the light flux propagation within the screen mass and may affect the spatial distribution of the light at the screen emitting surface, resulting in a significantly better MTF. The significance of this issue was verified by comparing a conventional Gd_2O_2S:Tb screen (packing density: 50%, grain size: 7 μm) with a non-conventional Gd_2O_2S:Tb screen (packing density:85%, grain size: 4 μm) of equal coating weight (31.7 mg/cm^2). Comparison was performed by applying a 30 kVp poly-energetic molybdenum x-ray spectrum, filtered by 0.051mm of molybdenum and 4.2 cm of Lucite. As shown in Fig. 13, by selecting a phosphor grain size of 4 μm and a packing density of 85%, a Gd_2O_2S: Tb screen may exhibit considerably higher MTF. Similar results were observed by comparing MTF data, assuming equal screen thickness (85 μm). In Fig. 14 are shown MTF curves indicating the superiority of the high packing density-small grain size Gd_2O_2S screen over the conventional Gd_2O_2S screens. In order to examine the light emission efficiency under similar conditions, results of light emitted photons per incident x-ray are also shown in Table VI. Results were obtained for the conventional Gd_2O_2S:Tb screen (packing density: 50%, grain size: 7 μm) as well as for the high packing density, small grain Gd_2O_2S:Tb screen (packing density: 85%, grain size: 4 μm). As it may be seen (e.g. at 49 keV x-ray energy), in addition to better resolution properties,

the high packing density-small grain size Gd_2O_2S:Tb screen also exhibits better light emission properties.

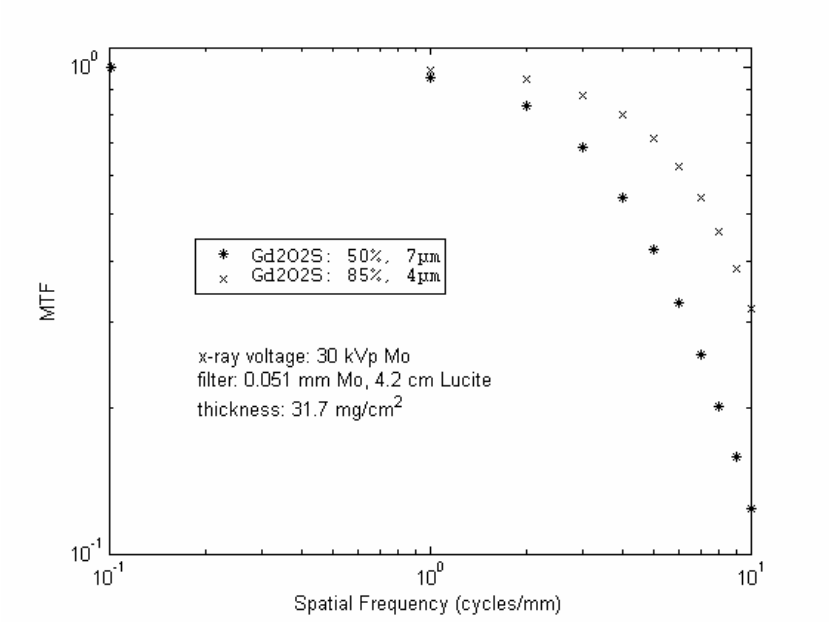

Figure 13. The variation of MTF as function of spatial frequency. Comparison between the conventional Gd_2O_2S:Tb screen (packing density 50%, grain size 7 μm) and the high packing density, small grain size Gd_2O_2S:Tb screen (packing density 85% and grain size 4 μm) with coating weight 31.7 mg/cm^2.

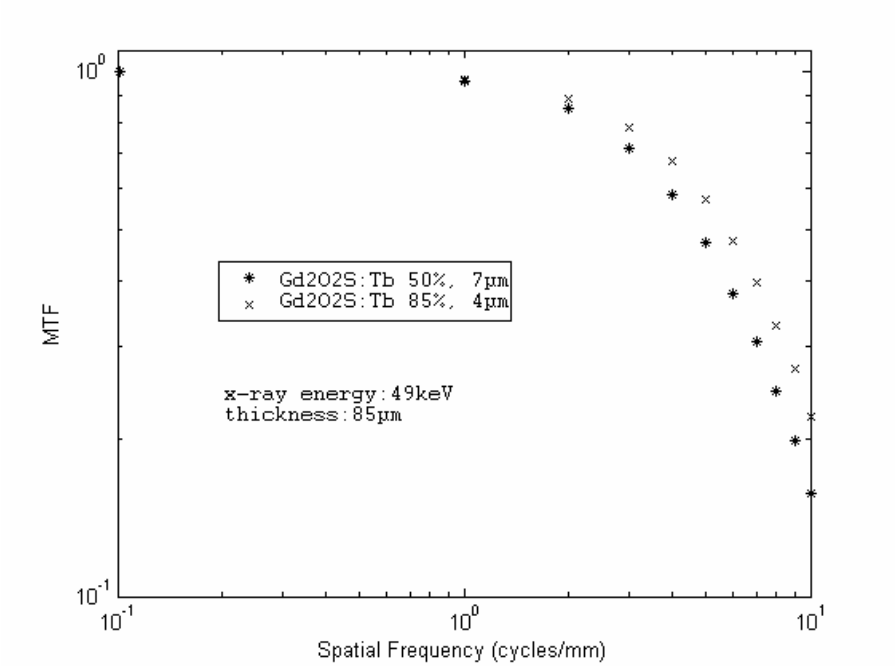

Figure 14. The variation of MTF as function of spatial frequency. Comparison between the conventional Gd_2O_2S:Tb screen (packing density 50%, grain size 7 μm) and the high packing density, small grain size Gd_2O_2S:Tb screen (packing density 85% and grain size 4 μm) with thickness 85 μm.

Table VI. Comparison of light emitted per incident x-ray between the conventional Gd_2O_2S:Tb screen (packing density 50%, grain size 7 μm) and the high packing density, small grain size Gd_2O_2S:Tb screen (packing density 85% and grain size 4 μm).

	Gd_2O_2S:Tb Phosphor thickness: 85 μm			
Incident energy (keV)	18	49	51	69
	Light emitted per incident x-ray (Front screen)			
Grain size: 7 μm Packing density: 50 %	275 ± 2	101 ± 5	192 ± 3	173 ± 5
Grain size: 4 μm Packing density: 85 %	244 ± 3	143 ± 5	294 ± 6	264 ± 7

An 85 μm thick Gd_2O_2S phosphor layer with 50% packing density corresponds to coating weight of 31.7 mg/cm^2. For 85% packing density, the corresponding coating weight is 53 mg/cm^2. This increases x-ray absorption and, therefore, the amount of light, initially created within the screen, is higher. However, light attenuation, determined by the number of light - phosphor grain interactions per unit of length, increases with packing density. Thus, light absorbed per light produced is higher, being approximately 5 % in the case of Gd_2O_2S:Tb (85%, 4 μm) instead of 0.5% in the case of Gd_2O_2S:Tb (50%, 7 μm). In conclusion, by increasing the packing density of a screen, the resolution (MTF) as well as the light emission properties become better. This may provide an advantage over techniques based on absorbing dyes incorporation for screen resolution improvement.

CHAPTER E

CONCLUSIONS, MODEL LIMITATIONS AND FUTURE WORK

There is no a complete knowledge that one day is going to be learned

E.1 Conclusions

A new computational model, based on Monte Carlo methods, has been developed to simulate the x-ray and light interaction mechanisms within granular phosphor screens. The model was validated with published experimental data and was used to perform the x-ray absorption and the light emission properties of powder screens in relation to x-ray energy. The model, by using the physical characteristics (complex refractive index, light wavelength) of the phosphor materials, applied Mie theory in order to describe light propagation. The effect of the material structure parameters (grain size, packing density) on light spread, as well on MTF was investigated. It was shown that these parameters were of crucial importance and can affect the number of light interactions, the angle of the scattered light (the anisotropy factor) and therefore the spatial resolution performance of phosphor screens. Granular screens of higher packing density and lower grain size were found to present considerably better light emission (approximately 1.5 times higher amount of emitted light) and spatial resolution properties (approximately MTF=0.22 instead of MTF=0.16 at 10 cycles/mm) in comparison with conventional screens, under similar conditions (e.g. equal x-ray energy and phosphor thickness).

E.2 Model limitations and Future work

The present PhD discourse deals with a detailed Monte Carlo simulation model applied in phosphor screens of medical imaging systems. The efficiency of the model has been analytically shown throughout the study. However, it may be of significance to note that the accuracy of our results are subject to limitations related to: (a) the model's dependence on tabulated physical data (i.e. index of refraction) and on data

drawn from the literature (i.e. light emission wavelength) (b) assumption of Poisson distribution for the production of light quanta per absorbed x-ray photon (c) assumption for monochromatic light photons (d) use of the common value (10^{-6}) for the imaginary part of the complex refractive index, (e) no reflection at the boundaries was considered, (f) the effect of secondary electron range was not considered (g) the afterglow exhibition was not taken into account.

General purpose for the future work is to extend the model in such away to overcome the aforementioned limitations. A series of simulations is needed to be done for a variety of phosphor materials. Data obtained will help to improve the performance of the model (i.e. some of the initial conditions may change) and new geometries and detector design could be achieved. Noise performance within granular screens of different values of packing density remains an opened issue of high interest.

APPENDIX A: X-RAY TRANSPORT

The mean photon free path length (fpl) and the interaction site co-ordinates of the x-ray photon are obtained as follows:

(a) ***A mean photon free path length***, fpl, was randomly sampled employing an inversion method from the corresponding probability distribution function (Chan and Doi 1983b) $P(fpl)$, which is an exponential function of fpl. This procedure is given as follows:

Let R_1 be a random number uniformly distributed in the interval (0, 1], such that $CDF(fpl) = R_5$, where $CDF(fpl)$ is the cumulative distribution function defined as:

$$CDF(fpl) = \int_0^{fpl} P(fpl)d(fpl) = R_5 \tag{A1a}$$

where

$$P(fpl) = \frac{\mu(E)}{\rho}\exp(-\frac{\mu(E)}{\rho}\rho_P fpl) \tag{A1b}$$

From (1a) and (1b) it may be obtained that:

$$fpl = \frac{\rho}{\mu(E)\rho_P}\ln R_5 \tag{A2}$$

where $\mu(E)$ is the linear attenuation coefficient of the phosphor material, ρ is the bulk density, and ρ_P is the packing density.

(b) ***The co-ordinates of the photon interaction site*** were calculated from the free path length and the direction of the x-ray photon, as it is given bellow:

$$\begin{pmatrix} x_{n+1} \\ y_{n+1} \\ z_{n+1} \end{pmatrix} = \begin{pmatrix} x_n \\ y_n \\ z_n \end{pmatrix} + fpl \begin{pmatrix} a \\ b \\ c \end{pmatrix} \tag{A3}$$

where $(x_{n+1}, y_{n+1}, z_{n+1})$, (x_n, y_n, z_n) are the coordinates of two successive interaction sites and (a,b,c) is a vector representing the direction cosines of the x-ray photon trajectory, given by $(a,b,c) = (\sin\theta\cos\phi, \sin\theta\sin\phi, \cos\theta)$. θ and ϕ are the polar and azimuthal angles, respectively, which were initially determined from the considered beam geometry. Each new interaction site was checked for lying outside the phosphor screen dimensions otherwise the x-ray photon was considered to interact with the phosphor material.

The type of interaction was determined by the relative probabilities of occurrence of each process. Setting a random number R_6, the choice of interaction was described as follows:

1) The probabilities of occurrence for each interaction were first calculated by the relations:

$$p_{PHOT} = \frac{\mu_{PHOT}}{\mu} \quad , \; p_{INC} = \frac{\mu_{INC}}{\mu} \quad , \; p_{COH} = \frac{\mu_{COH}}{\mu} \tag{A4}$$

where μ_{PHOT} , μ_{INC} , μ_{COH} are the partial interaction coefficients for the corresponding interaction: photoelectric effect, incoherent and coherent scattering, respectively.

2) The type of interaction (i) was then determined by relations (A5), where $i = 1, 2, 3$ implies photoelectric effect, incoherent scattering, and coherent scattering, respectively.

$$if \quad \begin{cases} 0 < R_6 \le \dfrac{p_{PHOT}}{p_{PHOT} + p_{INC} + p_{COH}} & then \quad i = 1 \\ \dfrac{p_{PHOT}}{p_{PHOT} + p_{INC} + p_{COH}} < R_6 \le \dfrac{p_{PHOT} + p_{INC}}{p_{PHOT} + p_{INC} + p_{COH}} & then \quad i = 2 \\ \dfrac{p_{PHOT} + p_{INC}}{p_{PHOT} + p_{INC} + p_{COH}} < R_6 \le 1 & then \quad i = 3 \end{cases} \tag{A5}$$

Once the type of interaction has been selected, this interaction (i) occurs to the j^{th} element of the phosphor material, according to the following probability (Chan and Doi 1983a):

$$p_i(Z_j,E)=\frac{w_j\left(\frac{\mu(Z_j,E)}{\rho}\right)_i}{\sum_{j=1}^{N} w_j\left(\frac{\mu(Z_j,E)}{\rho}\right)_i} \tag{A6}$$

where w_j is the fractional weight of the j element, $\left(\frac{\mu(Z_j,E)}{\rho}\right)_i$ is the mass coefficient of the j element for (i) interaction and N is the total number of elements in the phosphor material.

In the case that the interaction happens to be a scattering process, then the procedure of x-ray photon transport starts again from step (a). The new direction of the x-ray photon is decided according to the corresponding polar angle θ and azimuthal angle ϕ of the scattering process, which were sampled as it will be described for each scattering process, afterwards. The cosines of this new direction are transformed into a global (laboratory) coordinate system, as follows (Spyrou et al 1998):

$$\begin{pmatrix} a' \\ b' \\ c' \end{pmatrix} = \begin{pmatrix} \cos\phi\cos\theta & -\sin\phi & \cos\phi\sin\theta \\ \sin\phi\cos\theta & \cos\phi & \sin\phi\sin\theta \\ -\sin\theta & 0 & \cos\theta \end{pmatrix} \begin{pmatrix} a \\ b \\ c \end{pmatrix} \tag{A7}$$

where: $(a,b,c)=(\sin\theta\cos\phi,\sin\theta\sin\phi,\cos\theta)$ are the direction cosines of the x-ray photon trajectory before scattering, i.e. a coordinate system with origin at the interaction point and the z-axis along the initial photon direction, and $(a',b',c')=(\sin\theta'\cos\phi',\sin\theta'\sin\phi',\cos\theta')$ are the direction cosines in the global coordinate system (laboratory frame).

APPENDIX B: SAMPLING THE POLAR ANGLE OF COHERENT SCATTERING

The PDF of the polar deflection is given by (Chan and Doi 1983b):

$$P_\theta(\cos\theta) \equiv P_1(\cos\theta)P_2(u^2) = \frac{1}{2}\left(1+\cos^2\theta\right)\frac{F^2(u,Z)}{I(u^2_{\max})} \tag{B1}$$

where,

$$P_1(\cos\theta) = \frac{1}{2}\left(1+\cos^2\theta\right) \tag{B1a}$$

and

$$P_2(u^2) = \frac{F^2(u,Z)}{I(u^2_{\max})} \tag{B1b}$$

$I(u^2)$ is the integrated form factor, which can be derived from the tabulated form factors (Hubbell et al 1975) by numerical integration, as follows:

$$I(u^2) = \int_0^{u^2} F^2(u,Z)du^2 \tag{B2}$$

$I(u^2)$ depends only on u^2, as expressed by (B2). Setting two different sequences of random numbers R_7 and R_8, the cosine of the polar angle was sampled according to the following procedure:

(i) Calculate $u^2_{\max}$ corresponding to the photon energy E, as given by equation (5), and determine $I(u^2_{\max})$ by linear interpolation from the tabulated values $\left[I(u^2), u^2\right]$.

(ii) Determine $I(u^2)$ as follows:

$$I(u^2) = R_7 I(u^2_{\max}) \tag{B3}$$

(iii) Determine the random sample u^2, corresponding to the chosen $I(u^2)$, by linear interpolation from the tabulated values $\left[u^2, I(u^2)\right]$.

(iv) Determine $\cos\theta$ by the following equation:

$$\cos\theta = 1 - \left(\frac{um_0c^2}{29.1433E} \right)^2 \tag{B4}$$

(v) Calculate $P_1(\cos\theta)$ and test the corresponding rejection function (B1a).

If $R_8 \le P_1(\cos\theta)$ deliver $\cos\theta$, otherwise go to step (i).

APPENDIX C: SAMPLING THE POLAR ANGLE OF INCOHERENT SCATTERING

The PDF of the polar deflection is given by (Brusa et al 1996):

$$P_\theta(\cos\theta) = \left(\frac{E_C}{E}\right)^2 \left(\frac{E_C}{E} + \frac{E}{E_C} - \sin^2\theta\right) S(E,\theta) \tag{C1}$$

The proposed sampling algorithm was described by the following procedure:

Let us consider the quantity

$$\tau \equiv \frac{E_C}{E} = \frac{1}{1 + k(1-\cos\theta)} \tag{C2}$$

where $k \equiv E/m_o c^2$. The minimum and maximum values of τ correspond to

$\cos\theta = -1$

and $\cos\theta = 1$, respectively, and are given by:

$$\tau_{\min} = \frac{1}{1+2k} \quad \text{and} \quad \tau_{\max} = 1 \tag{C3}$$

Using the combined composition and rejection (Rubinstein 1981) Monte Carlo methods the PDF can be rewritten in the following form:

$$P_\tau \tau = [a_1 P_1(\tau) + a_2 P_2(\tau)] T(\cos\theta) \tag{C4}$$

where

$$a_1 = \ln\left(\frac{1}{\tau_{\min}}\right),\ a_2 = \left(\frac{1-\tau_{\min}^{\ 2}}{2}\right),\ P_1(\tau) = \left(\frac{1}{a_1\tau}\right),\ P_2(\tau) = \left(\frac{\tau}{a_2}\right) \tag{C5}$$

and

$$T(\cos\theta) \equiv g(\cos\theta)\frac{S(E,\theta)}{S(E,\theta=\pi)} = \left(1 - \frac{\tau}{1+\tau^2}\sin^2\theta\right)\frac{S(E,\theta)}{S(E,\theta=\pi)} \tag{C6}$$

The function $g(\cos\theta)$ equals to unity at the end points of the interval $(\tau_{\min},1)$ and it is less than unity inside the interval. Setting four sequences of random

numbers R_9, R_{10}, R_{11} and R_{12}, the cosine of polar angle is sampled according to the following procedure:

(i) Sample a value of τ by the inversion method either from the CDF of $P_1(\tau)$ or $P_2(\tau)$ according to the corresponding point probabilities:

$$\pi(1) = \frac{a_1}{a_1 + a_2} \text{ and } \pi(2) = \frac{a_2}{a_1 + a_2} \tag{C7}$$

if $R_9 \le \pi(1)$ then $R_{10} = \int_{\tau\,\min}^{\tau} P_1(\tau) d\tau \Rightarrow \tau = \tau_{\min} \exp(R_{10} a_1)$, (C8)

otherwise $R_{10} = \int_{\tau\,\min}^{\tau} P_2(\tau) d\tau \Rightarrow \tau = \sqrt{\tau_{\min}^2 + 2R_{10}} a_2$ (C9)

(ii) Determine $\cos\theta$ from equation (C2) as given below:

$$\cos\theta = 1 - \frac{1-\tau}{k\tau} \tag{C10}$$

(iii) Calculate $g(\cos\theta)$ and test the first rejection function. If $R_{11} \le g(\cos\theta)$ deliver $\cos\theta$, otherwise go to step (i).

(iv) Calculate $\frac{S(E,\theta)}{S(E,\theta=\pi)}$ and test the second rejection function. If $R_{12} \le \frac{S(E,\theta)}{S(E,\theta=\pi)}$ deliver $\cos\theta$, otherwise go to step (i).

APPENDIX D: MIE THEORY

Light absorption and scattering coefficients m_{abs}, m_{sct} are given by the following equations:

$$m_{abs} = V_d A Q_{abs} \qquad \text{and} \qquad m_{sct} = V_d A Q_{sct} \tag{D1}$$

where each coefficient depends on the volume density of phosphor screen V_d, the geometrical cross-section A of the grain, as well as on the corresponding absorption Q_{abs} and scattering Q_{sct} efficiency factors, which are given below (Morlotti 1975, Van de Hulst 1957, Hong Du 2004):

$$Q_{ext} = \frac{2}{x^2}\sum_{n=1}^{\infty}(2n+1)\mathrm{Re}(a_n + b_n), \quad Q_{sct} = \frac{2}{x^2}\sum_{n=1}^{\infty}(2n+1)\left(|a_n|^2 + |b_b|^2\right) \tag{D2}$$

The geometrical cross-section of the grain A is proportional to the diameter of the grain d being equal to $A = \pi d^2/4$. The extinction and scattering efficiency factors are obtained from Mie calculations using the size parameter $x = \pi d n_{medium}/\lambda$ of Mie theory and the relative complex refractive index $m = n_{grain}/n_{medium}$, where λ is the wavelength of light, n_{grain} is the complex refractive index of the phosphor grains and n_{medium} is the refractive index of the of the medium. Finally, a_n and b_n are the so-called Mie coefficients, which are given by the following equations (Van de Hulst 1957):

$$a_n = \frac{\psi_n'(mx)\psi_n(x) - m\psi_n(mx)\psi_n'(x)}{\psi_n'(mx)\zeta_n(x) - m\psi_n(mx)\zeta_n'(x)}, \quad b_n = \frac{m\psi_n'(mx)\psi_n(x) - \psi_n(mx)\psi_n'(x)}{m\psi_n'(mx)\zeta_n(x) - \psi_n(mx)\zeta_n'(x)} \tag{D3}$$

where $\psi_n(x)$ and $\zeta_n(x)$ are the Riccati-Bessel functions. The calculation of these functions can be carried out by the following recurrences, taking into account their corresponding properties:

$$\psi_{n+1}(x) = (2n+1)\psi_n(x)/x - \psi_{n-1}(x)$$

$$\zeta_{n+1}(x) = (2n+1)\zeta_n(x)/x - \zeta_{n-1}(x)$$

$$\psi_n^{'}(x) = \psi_{n-1}(x) - n\psi_n(x)/x$$

$$\zeta_n^{'}(x) = \zeta_{n-1}(x) - n\zeta_n(x)/x$$

$$\psi_{-1}(x) = \cos(x) \ , \ \psi_0(x) = \sin(x)$$

$$\zeta_{-1}(x) = \cos(x) - i\sin(x) \ , \ \zeta_0(x) = \sin(x) + i\cos(x) \qquad \text{(D4)}$$

The infinite summations in relations (D2) for the extinction and scattering efficiency factors calculations converge after a certain number $N_{\max} = x + cx^{1/3} + b$, where c=4 and b=2 depending on x. Usually the recursion formulas are used up to $N_{\max}$ th order.

APPENDIX E: HENYEY-GREENSTEIN DISTRIBUTION

The probability density function of Henyey-Greenstein distribution (Peters et al 1990), $p(\cos\theta)$, is given below:

$$p(\cos\theta) = \frac{1-g^2}{2\left(1+g^2-2g\cos(\theta)\right)^{3/2}} \tag{E1}$$

where g is the anisotropy factor and corresponds to the mean cosine of the scattering angle (Peters et al 1990). Using the cumulative density function:

$$P(\cos\theta) = \int_{-1}^{\cos\theta} \frac{1-g^2}{2\left(1+g^2-2g\cos(\theta)\right)^{3/2}} d\cos\theta \tag{E2}$$

the random numbers of $\cos\theta$ are produced from the following equation (Peters et al 1990):

$$\cos\theta = \frac{1}{2g}\left[1+g^2-\left(\frac{1-g^2}{1-g+2gR}\right)^2\right] \quad \text{when} \quad g \neq 0 \tag{E3}$$

The free parameter g is the anisotropy factor, which implies isotropic distribution of light for $g = 0$ and sharply forward direction of light for $g = 1$. The anisotropy factor was calculated using the following equation (Van de Hulst 1957, Peters et al 1990):

$$g = \frac{\int_0^{\pi} 2\pi S_{11}(\theta)\cos\theta\sin\theta d\theta}{\int_0^{\pi} 2\pi S_{11}(\theta)\sin\theta d\theta} \tag{E4}$$

where $S_{11}(\theta)$ is the first element of the Mueller matrix(Van de Hulst 1957), which implies that light extinction is independent of the light polarization state. In numerical evaluation of the above expression for g, a large number of angles are required to be calculated in order to obtain a high precision value of g. $S_{11}(\theta)$ is associated to the

complex elements of scattering matrix $S_1(\theta)$ and $S_2(\theta)$ as follows (Bohren and Huffman 1983, Hong Du 2004):

$$S_{11}(\theta) = \left|S_1(\theta)\right|^2 + \left|S_2(\theta)\right|^2 \tag{E5}$$

where

$$S_1(\theta) = \sum_{n=1}^{\infty} \frac{2n+1}{n(n+1)} \left(a_n \pi_n(\cos\theta) + b_n \tau_n(\cos\theta)\right) \tag{E6}$$

and

$$S_2(\theta) = \sum_{n=1}^{\infty} \frac{2n+1}{n(n+1)} \left(b_n \pi_n(\cos\theta) + a_n \tau_n(\cos\theta)\right) \tag{E7}$$

The angle-dependent functions π_n and τ_n were computed by upward recurrence from the following relations:

$$\pi_n = \frac{2n-1}{n-1} \cos\theta \pi_{n-1} - \frac{n}{n-1} \pi_{n-2} \tag{E8a}$$

and

$$\tau_n = n\cos\theta \pi_n - (n+1)\pi_{n-1} \tag{E8b}$$

beginning with $\pi_0 = 0$ and $\pi_1 = 1$.

APPENDIX F: ABBREVIATIONS

a-Si:H	Amorphous-silicon
CDF	Cumulative Distribution Function
DQE	Detective Quantum Efficiency
DR	Digital radiography
EAE	Energy Absorption Efficiency
FFT	Fast Fourier Transform
fpl	free path length
Gd_2O_2S:Tb	Gadolinium oxy-sulphide
LE	Light Efficiency
LSF	Line Spread Function
MC	Monte Carlo
Mo	Molybdenum
MTF	Modulation transfer function
PDF	Probability Density Function
PSD	Position-sensitive detector
PSF	Point Spread Function
QDE	Quantum Detection Efficiency
rms	root mean square
SF	Swank Factor
TH	Theoretical

REFERENCES

1. Aerts W., De Meester P. J. and Bollen R., "A Monte Carlo simulation of complete systems for radiographic image registration," Mater. Eval. **40**, 1071-1075 (1982).
2. Alig R. C. and Bloom S., "Cathodoluminescent Efficiency," J. Electrochem. Soc. **124**, 1136-1138 (1977).
3. Andreo P, "Monte Carlo techniques in medical radiation physics," Phys. Med. Biol. **36**, 861-920 (1991).
4. Badano A., Gagne R. M., Gallas B. D., Jennings R. J., Boswell J. S. and Myers K .J., "Lubberts effect in columnar phosphors," Med. Phys. **31**, 3122-3131 (2004).
5. Berger M. J., Hubell J. H., Seltzer S. M., Coursey J. S., Zucker D. S., XCOM: Photon cross section database. Technical report, NIST, (1999). http://physics.nist.gov/xcom.
6. Beutel J., Apple B. A. and Shaw R., "The role of screen parameters and print-through in the performance of film/screen systems," Phys. Med. Biol. **38**, 1181-1193, (1993).
7. Beutel J. and Kittis E. L., "The image quality characteristics of a novel film/screen system for mammography," Proc. SPIE **2708**, 233-240, (1996).
8. Blasse G., "The luminescent efficiency of scintillators for several applications: state-of-the-art," Jour.of. Lum. **60&61**, 930-935 (1994).
9. Blasse G. and Grabmaier B. C., *Luminescent materials* (Spinger, Berlin, 1994).
10. Bohren C. F. and Huffman D. R., *Absorption and Scattering of Light by Small Particles* (Wiley, New York, 1983).

11. Boone J. M., "Spectral modeling and compilation of quantum fluence in radiography and mammography," Proc. SPIE 3336, 592-601, (1998). X-ray simulation tool.
http://www.med.siemens.com/med/rv/spektrum/default.asp
12. Boone J. M. and Chavez A. E., "Comparison of x-ray cross sections for diagnostic and therapeutic medical physics," Med. Phys. **23**, 1997-2005 (1996).
13. Boone J. M., Fewell T. R. and Jennings R. J., "Molybdenum, rhodium, and tungsten anode spectral models using interpolating polynomials with application to mammography," Med. Phys. **24**, 1863-1874, (1997). X-ray simulation tool.
http://www.med.siemens.com/med/rv/spektrum/default.asp
14. Boone J. M. and Seibert A., "An accurate method for computer-generating tungsten anode X-ray spectra from 30 to 140 kV," Med. Phys. **24**, 1661-1670, (1997).X-ray simulation tool.
http://www.med.siemens.com/med/rv/spektrum/default.asp
15. Boone J. M. and Seibert J. A., "A Monte Carlo study of x-ray fluorescence in x-ray detectors," Med. Phys. **26**, 905-916 (1999).
16. Brusa D., Stutz G., Riveros J. A., Fernandez-Varea J. M. and Salvat F., "Fast sampling algorithm for the simulation of Compton scattering" Nucl. Instrum. Meth. A **379**, 167-175, (1996).
17. Bunch P. C., Huff K. E., and Van Metter R., "Analysis of the detective quantum efficiency of a radiographic screen-film combination," J. Opt. Soc. Am. **4**, 902-908, (1987).
18. Chan H. P. and Doi K., "Energy and angular dependence of x-ray absorption and its effect on radiographic response in screen-film systems," Phys. Med. Biol. **28**, 565-579 (1983).

19. Chan H. P. and Doi K., "The validity of Monte Carlo simulation in studies of scattered radiation in diagnostic radiology," Phys. Med. Biol. **28**, 109-129 (1983).
20. Cullen D. E., Hubbell J. H. and Kissel L., 'EPDL97 The evaluated data library, '97 version', Report UCRL-50400, LLNLL, CA, (1997).
21. Derenzo S. E., Moses W. W., Cahoon J. L.,. Perera R. C. C and Litton J. E., "Prospects for new inorganic scintillators," IEEE Trans. Nucl. Sci. **NS-37**, 203-208 (1990).
22. Dick C. E. and Motz J. W., "Image information transfer properties of x-ray fluorescent screens," Med. Phys. **8**, 337-346 (1981).
23. Dick C. E. and Motz J. W., "Utilization of monoenergetic x-ray beams to examine the properties of radiographic intensifying screens," IEEE Trans. Nucl. Sci. **NS-28**, 1554-1558 (1981).
24. Gallas B. D., Boswell J. S., Badano A., Gagne R. M., and Myers K .J., "An energy- and depth-dependent model for x-ray imaging," Med. Phys. **31**, 3132-3149 (2004).
25. Giakoumakis G. E., Katsarioti M. C., Lagaris I. E. and Panayiotakis G. S., "A theoretical model for the x-ray luminescence of granular phosphor screens," J. Appl. Phys. **69**, 6607-6610 (1991).
26. Giakoumakis G. E. and Nomicos C. D., "Light angular distribution of non-granular fluorescent screens excited by x-rays," Phys. Med. Biol. **30**, 993-1003 (1985).
27. Giakoumakis G. E., Nomicos C. D. and Euthimiou P. C., "Modulation transfer function of fluorescent screens excited by x-rays," Phys. Med. Biol. **25**, 1105-1110 (1980).

28. Giakoumakis G. E., Nomicos C. D., Yiakoumakis E. N. and Evangelou E. K., "Absolute efficiency of rare earth oxysulphide screens in reflection mode observation" Phys. Med. Biol. **35**,1017-1023 (1990).
29. Ginzburg A. and Dick C. E., "Image information transfer properties of x-ray intensifying screens in the energy range from 17 to 320 keV," Med. Phys. **20**, 1013-1021 (1993).
30. Graaff R., Koelink M. H., de Mul F. F. M.,. Zijlstra W. G, Dassel A. C. M. and Aarnoudse J. G., "Condensed Monte Carlo simulations for the description of light transport," Appl. Optics. **32**, 426-434 (1993).
31. Gruner S. M., Tate M. W. and Eikenberry E. F., "Charge-coupled device area x-ray detectors," Rev. Sci. Instur. **73**, 2816-2842 (2002).
32. Hamaker H., "Radiation and heat conduction in light-scattering material," Philips Res. Rep. **2**, 55-67 (1947).
33. Hong Du, "Mie-scattering calculation," Appl. Optics **43**, 1951-1956 (2004).
34. Hubbell J. H., Trehan P. N., Nirman Singh, Chand B., Mehta D.,. Garg M. L, Grag R. R., Surinder Singh and Puri S., "A review, bibliography, and tabulation of K, L, and higher atomic shell x-ray fluorescence yields" J. Phys. Chem. Ref. Data **23** , 339-364, (1994).
35. Hubbell J. H., Veigele Wm. J., Briggs E. A., Brown R. T., Cromer D. T. and Howerton R. J., "Atomic form factors, incoherent scattering functions, and photon scattering cross sections" J. Phys. Chem. Ref. Data. **4**, 471-537, (1975).
36. Jaffray D. A., Battista J. J., Fenster A. and Munro P., "Monte Carlo studies of x-ray energy absorption and quantum noise in megavoltage transmission radiography," Med. Phys. **22**, 1077-1088 (1995).

37. Johns H. E. and Cunningham J. R, *The physics of radiology* (Thomas, Springfield, IL, 1983).

38. Kalender W., "Monte Carlo calculations of x-ray scatter data for diagnostic radiology," Phys. Med. Biol. **26**, 835-849 (1981).

39. Kandarakis I., Cavouras D., Panayiotakis G. S. and Nomicos C. D., "Evaluating x-ray detectors for radiographic applications:A comparison of ZnSCdS:Ag with Gd_2O_2S:Tb and Y_2O_2S:Tb screens," Phys. Med. Biol. **42**, 1351-1373 (1997).

40. Kausch C., Schreiber B., Kreuder F., Schmidt R. and Dössel O. "Monte Carlo simulations of the imaging performance of metal plate/phosphor screens used in radiotherapy," Med. Phys. **26**, 2113-2124 (1999).

41. Knoll G. F., *Radiation Detection and Measurement*, 2nd ed. (Wiley, New York,1989).

42. Lindstrom J. and Carlsson G. A., "A simple model for estimating the particle size dependence of absolute efficiency of fluorescent screens," Phys. Med. Biol. **44**, 1353-1367 (1999).

43. Ludwig G. W., "X-ray efficiency of powder phosphors," J. Electrochem. Soc. **118**, 1152-1159 (1971).

44. Ludwig G. W. and Prener J. S., "Evaluation of Gd_2O_2S:Tb as a phosphor for the input screen of x-ray image intensifier," IEEE Trans. Nucl. Sci. **13**, 3-8 (1972).

45. Morin R. L., *Monte Carlo simulation in the radiological science* (CRC Press, 1988).

46. Morlotti R., "X-ray efficiency and modulation transfer function of fluorescent rare earth screens, determined by the Monte Carlo method," J. Photogr. Sci. **23**, 181-189 (1975).

47. Morlotti R., Nicl M., Piazza M., Boragno C., "Intrinsic conversion efficiency of X-rays to light in $Gd_2O_2S:Tb^{3+}$ powder phosphors," Jour.of. Lum. **72-74**, 772-774 (1997).

48. Moy J-P., "Recent developments in x-ray imaging detectors," Nucl. Instrum. Meth. A **442**, 26-37, (2000).

49. Nagarkar V. V., Miller S. R., Tipnis S. V., Lempicki A., Brecher C. and Lingertat H., "A new large area scintillator screen for X-ray imaging," Nucl. Instrum. Meth. B **213**, 250-254 (2004).

50. Nielsen B. and Carlson C. A., "Energy imparted to fluorescent screens from primary and scattered radiation. Variations with atomic composition and screen thickness," Phys. Med. Biol. **29**, 315-328 (1984).

51. Nishikawa R. M. and Yaffe M. J., "Model of the spatial-frequency-dependent detective quantum efficiency of phosphor screens," Med. Phys. **17**, 894-904 (1990).

52. Peters V. G., Wyman D. R., Patterson M. S. and Frank G. L., "Optical properties of normal and diseased human breast tissues in the visible and near infrared," Phys. Med. Biol. **35**, 1317-1334 (1990).

53. Radcliffe T., Barnea G., Wowk B., Rajapakshe R., and Shalev S. "Monte Carlo optimization of metal/phosphor screens at megavoltage," Med. Phys. **20**, 1161-1169 (1993).

54. Raeside D. E., "Monte Carlo principles and applications," Phys. Med. Biol. **21**, 181-197 (1976).

55. N.T.Ranger, E. Samei, J. T. Dobbins, C. E. Ravin, "Measurement of the detective quantum efficiency in digital detectors consistent with the IEC 62220-

1 standard: Practical considerations regarding the choice of filter material," Med. Phys. **32**, 2305-1311 (2005).

56. Roos A. and Ronnow D., "Diffuse reflectance and transmittance spectra of an interference layer: 1. Model formulation and properties," Appl. Optics **33**, 7908-7917 (1994).
57. Rubinstein R. Y., *Simulation and the Monte Carlo method,* (Wiley, New York, 1981).
58. Sempau J., Acosta E., Baro J., Fernandez-Varea J. M. and Salvat F., "An algorithm for Monte Carlo simulation of coupled electron-photon transport," Nucl. Instrum. Meth. B **132**, 377-390 (1997).
59. Spyrou G., Tzanakos G., Bakas A. and Panayiotakis G., "Monte Carlo generated mammograms: development and validation," Phys. Med. Biol. **43**, 3341-3357 (1998).
60. Swank R. K., "Absorption and noise in x-ray phosphors," J. Appl. Phys. **45**, 4199-4203 (1974).
61. Van de Hulst H. C., *Light Scattering by Small Particles* (Wiley, New York, 1957).
62. Van Eijk C. W E., "Inorganic-scintillator development" Nucl. Instrum. Meth. A **460**, 1-14 (2001).
63. Van Eijk C. W. E, "Inorganic scintillators in medical imaging," Phys. Med. Biol. **47**, R85-R106 (2002).
64. Venema H. W., "X-ray absorption, speed and luminescent efficiency of rare earth and other intensifying screens," Radiology. **130**, 765-771 (1979).

65. Wang L., Jacques S. L., Zheng L., "MCML-Monte Carlo modeling of light transport in multi-layered tissues," Comput. Meth. Prog. Bio. **47**, 131-146 (1995).

66. Yaffe M. J., "Physics and Psychophysics" *Handbook of Medical Imaging* (SPIE, 2000), edited by J. Beutel, H. L. Kundel and R. L. Van Metter, Vol. I, Chap. 5. pp. 329-372.

67. Yaffe M. J. and Rowlands J. A, "X-ray detectors for digital radiography," Phys. Med. Biol. **42**, 1-39 (1997).

68. Zaidi H., "Comparative evaluation of photon cross-section libraries for materials of interest in PET Monte Carlo simulations" IEEE Trans. Nucl. Sci. **47**, 2722-2735 (2000).

69. W. Zhao, G. Ristic and J. A. Rowlands, "X-ray imaging performance of structured cesium iodide scintillators" Med. Phys. **31**, 2594-2605 (2004).